# A Novel lncRNA ARST Represses Glioma Progression by Inhibiting ALDOA-mediated Actin Cytoskeleton Integrity

**Jun Sun**
Shandong University Cheeloo College of Medicine
**Dong He**
Shandong University Cheeloo College of Medicine
**Yibing Fu**
Shandong Provincial Hospital
**Rui Zhang**
Shandong Provincial Hospital
**Hua Guo**
Shandong Provincal Hospital
**Zhaojuan Wang**
Shandong Medical College
**Yanan Wang**
Taian Municipal Hospital
**Taihong Gao**
Shandong Provincial Hospital
**Yanbang Wei**
Shandong University Cheeloo College of Medicine
**Yuji Guo**
Shandong University Cheeloo College of Medicine
**Qi Pang** ( pangqi@sdu.edu.cn )
Department of Neurosurgery, Shandong Provincial Hospital, Cheeloo College of Medicine, Shandong University, Jinan 250012, Shandong, P. R. China
**Qian Liu**
Shandong

---

**Research**

**Keywords:** LncRNA, Glioma, ARST, ALDOA, Actin Cytoskeleton

**Posted Date:** December 17th, 2020

**DOI:** https://doi.org/10.21203/rs.3.rs-125314/v1

# Abstract

**Background:** Glioma is one of the most aggressive malignant brain tumors that is characterized with highly infiltrative growth and poor prognosis. ARST is a novel lncRNA which expression is significantly decreased in the patients with glioblastoma multiforme. However, the exact mechanisms of ARST in gliomagenesis are largely unknown.

**Methods:** The expressions of ARST in the glioma samples and cell lines were analyzed by qRT-PCR. FISH was utilized to detect the distribution of ARST in the glioma cells. CCK-8, EdU and flow cytometry were used to examine cellular viability, proliferation and apoptosis. Transwell and wound-healing assays were performed to determine the migratory and invasive abilities of the cells. Intracranial tumorigenesis models were established to explore the roles of ARST in vivo. RNA pulldown assay was used to examine proteins that bound to ARST. The activities of key enzymes in the glycolysis and production of lactate acid were measured by colorimetry. In addition, RIP, Co-IP, western blot, immunofluorescence were used to investigate the interaction and regulation between ARST, F-actin, ALDOA and cofilin.

**Results:** In this study, we reported that ARST was downregulated in the gliomas. Overexpression of ARST in the glioma cells significantly suppressed various cellular vital abilities such as cell growth, proliferation, migration and invasion. The tumorigenic capacity of these cells in vivo was reduced as well. We further demonstrated that the tumor suppressive effects of ARST could be mediated by a direct binding to a glycolytic enzyme aldolase A (ALDOA), which together with cofilin, keeps the polymerization and depolymerization of actin filaments in an orderly dynamic equilibrium. Upregulation of ARST interrupted the interaction of ALDOA and actin cytoskeleton, which led to a rapid cofilin-dependent loss of F-actin stress fibers.

**Conclusions:** Taken together, it is concluded that ARST performs its function via a non-metabolic pathway associated with ALDOA, which otherwise modifies the morphology and invasive properties of the glioma cells. This has added new perspective to its role in tumorigenesis, thus providing potential target for glioma diagnosis, therapy, and prognosis.


# Background

Gliomas are the most common and aggressive malignant brain tumors, which account for 30% of all central nervous system tumors and 80% of all primary malignant brain tumors [1]. They are characterized with highly infiltrative growth, making them elusive targets for effective surgical management and leading to tumor recurrence. According to the pathology, Gliomas are classified into four grades: Ⅰ, Ⅱ, Ⅲ and Ⅳ [2]. Glioblastoma (GBM) is the most severe glioma type that belongs to Grade Ⅳ. Another types, Grade Ⅰand Ⅱ, are referred to as low grade gliomas (LGGs). Despite advances in neuro-oncology to optimize treatment options, the prognosis of patients with gliomas still remains poor. Therefore, it is critical to understand the pathogenesis of gliomas and explore new effective therapeutic targets for better clinical inventions.

Recently, the roles of non-coding RNAs (ncRNAs) in tumors have attracted increasing attentions [3], among which long non-coding RNAs (lncRNAs) are a diverse and poorly conserved category of RNAs [4]. Longer than 200 nucleotides, they have demonstrated crucial roles in the transcriptional and post-transcriptional regulation of gene expression [5]. Nowadays, accumulating evidences have indicated close involvement of lncRNAs in cancer pathogenesis, including gliomas. For instance, lncRNA MIR22HG is a critical inducer of the Wnt/β-catenin signalling pathway. Targeting lncRNA MIR22HG may represent a novel therapeutic strategy in glioma patients [6]. What's more, lncRNA HOTAIR which is contained in the serum-derived exosomes can also be used as a novel prognostic and diagnostic biomarker for GBM [7]. Until now, more and more glioma-associated lncRNAs have been discovered, however their functions and regulatory mechanisms are still elusive.

Fructose-bisphosphate aldolase A (ALDOA) is one of the key enzymes in glycolysis. Since the most well-known and prevalent metabolic change associated with cancer cells is enhanced aerobic glycolysis, ALDOA is often found to be highly expressed and act as an oncogene in many types of cancers such as renal clear cell, hepatocellular and lung squamous cell carcinomas [8–10]. What's more, the increasing level in ALDOA expression is positively correlated with the degree of malignancy and inversely correlated with the prognosis. Most remarkably, the latest research propose that some glycolytic enzymes reveal moonlighting roles that are unrelated to glycolysis and they act as regulators of a variety of cellular processes. ALDOA, for instance, plays an important role in the polymerization of actin cytoskeleton [11].

Actin filaments are one of the key elements of cytoskeleton, the integrity of which is crucial for various cellular processes such as proliferation, migration, invasion and apoptosis [12]. In normal circumstances, a dynamic equilibrium state is maintained between depolymerization of old actin filaments and polymerization of new fibers, the cycle of which contributes to the migration and invasion of the cells [13, 14]. Recent studies have clarified that ALDOA could promote F-actin polymerization by interacting with γ-actin. Blocking the interaction between ALDOA and γ-actin reversed this polymerization to G-actin [15]. On the other hand, cofilin, an actin depolymerization protein (ADP), plays an important role in the depolymerization of actin cytoskeleton [11, 15]. The subsequent release of G-actin monomers would be used to promote the assembly of new F-actin fibers. However, the detailed molecular regulatory mechanisms of this process still need further investigations.

In this study, we reported a novel lncRNA, ALDOA related specific transcript (ARST) which was downregulated in the gliomas. Overexpression of ARST in the glioma cells interrupted the interaction between ALDOA and F-actin cytoskeleton, which led to a rapid cofilin-dependent loss of F-actin stress fibers. Various cellular vital abilities such as cell growth, proliferation, migration and invasion were inhibited as well. This research demonstrated for the first time that ARST acts as a tumor suppressor in gliomas by a non-metabolic pathway associated with ALDOA, which may be a potential therapeutic target for glioma diagnoses, therapies, and prognoses.

# Methods

# High throughput sequencing analysis and data arrangement

Using high throughput sequencing technique, we defined the clusters of differential expressing LncRNAs in the glioma specimens and paracarcinomic tissues. The suffix E-Signal represented the paracarcinomic tissues, and the suffix T-Signal represented the tumor tissues. Clusters in green indicated the downregulated LncRNAs and clusters in red indicated the opposite.

# Clinical samples and cell lines

A total of 144 specimens were collected from tumorectomy of gliomas in the Department of Neurosurgery, Shandong Provincal Hospital Affiliated to Shandong University, Jinan. The adjacent brain tissue was defined as 1 cm away from the lesions. The criteria for the inclusion/exclusion of patient are: (1) age 0–70; (2) only received surgeries, without preoperative chemotherapies or radiation therapies; (3) without other types of cancers, autoimmune diseases, infectious diseases, etc. All specimens were obtained under sterile conditions during surgeries, snap frozen in liquid nitrogen, and stored at 80 °C. The corresponding clinical data were also obtained. This study was approved by the Human Ethics Committee of Hospital. The individuals were informed about the study and gave consent prior to the specimen collection.

We selected human glioma cell lines U87MG and U251, normal human astrocytes (NHA) and mouse glioma cell line GL261 as our experimental cell lines, provided from Shanghai Institutes for Biological Sciences Cell Resource Center (Shanghai, China).

# Cell culture and transfection

The cell lines were cultured in DMEM medium with high glucose and sodium pyruvate, supplied with 10% fetal bovine serum, 100 units/mL penicillin and 100 μg/mL streptomycin. The culturing environmental condition was 37℃ with 5% CO2. Transfections of SMART silencer RNA (RiboBio, Guangzhou, China) and overexpression plasmids were performed using Lipofectamine 2000 (Invitrogen). Plasmid extracting was performed by OMEGA Endo-free Plasmid Mini Kit II (D6950-01, Shanghai, China), according to the manufacturer's instructions. The glycerol bacteria containing mutating peptide of ALDOA was produced by Jinan Boshang Biotechnology Limited Company. Detailed transfection procedures were referred to the instructions.

# RNA fluorescence in situ hybridization (FISH) assay

In order to detect subcellular localization of lncRNA ARST, we utilized Fluorescence in Situ Hybridization Kit (Cat.10910) (RiboBio, Guangzhou, China). Procedures were described previously [16]. The probes were also designed and synthesized by RiboBio, Guangzhou. U87MG and U251 were selected for the experiments. The hybridization step needed to be placed in 42℃ overnight with enough humidity.

# RNA isolation and quantitative reverse transcription PCR (qRT-PCR) assay

Experimental related primers were designed and produced by Takara, Japan. Cellular total RNA was isolated and concentrated by TransZol Up (Lot#10315) (Transgen, Beijing, China). The primer sequences are listed as follows. ARST: 5'-TCAGCGCATAGCTCAAGTCT-3' (forward), ARST: 5'-GGTAGGCTCTTCTCAGGCAC-3' (reverse); ALDOA: 5'-ATGCCCTACCAATATCCAGCA-3' (forward), and ALDOA: 5'-GCTCCCAGTGGACTCATCTG-3' (reverse). qRT-PCR assay was performed using the TransStart Tip Green qPCR SuperMix Kit (Transgen, Beijing, China) and CFX Connect Real-time PCR System (Applied Bio-rad, USA) according to the manufacturer's instructions. gDNA was removed and cDNA was reversed transcribed by TransScript One-Step gDNA Removal and cDNA synthesis SuperMix (Lot#L20602) (Transgen, Beijing, China). 500 ng cDNA, the forward and the reverse primers, the reaction mixture were used to amplify the PCR products corresponding to the human gene. The experiments were repeated at least three times independently to ensure the reproducibility of the results. Human β-actin and GAPDH were amplified as the internal controls. Comparative quantification was done by using the $2 - \Delta\Delta Ct$ method.

# Cell proliferation assay

Cells were planted in 96-well plates at the density of 2000 cells per well for 48 h. Cell viability was determined using the Cell Counting Kit-8 (CCK-8) (CK04, Dojindo, Japan). Procedures were described previously [17]. Optical density value was measured at 450 nm on iMark Microplate Reader (Bio-Rad, USA). Each group was set three replicated wells and CCK-8 assay was performed in three independently repeated experiments. EdU assay was performed by Cell-Light™ EdU Apollo567 In Vitro Imaging Kit (Ribobio, Guangzhou, China). The EdU assay was conducted as described previously [18].

# Wound-healing and transwell assays

Wound healing assay was performed on 6-well cell culture plates (Corning, USA). Scratching step was vertical performed on the center of each well, using 200 ul pipettes. Culturing for 12 h and 24 h in high glucose DMEM medium without fetal bovine serum (FBS). The figures were obtained on the microscope at 200×. The gap distance was measured by the plotting scale of software. The proportion of changes were calculated and analyzed in statistics. Transwell assay was applied for invasion and migration tests. Glioma cells were planted on the cell culture inserts in the 24-well plates (Corning, USA). For invasion test we used matrigel (BD Biosciences, USA). Cells were cultured in 100 ul serum-free DMEM in the upper chamber and 500 ul medium supplemented with 20% FBS in the lower chamber. After 6 h of incubation, the cells underside of the membrane were fixed, stained with crystal violet for 45 min, and counted under microscope.

# Flow cytometry assay

Annexin V-FITC apoptosis detection kit (Beyotime Biosciences, Shanghai, China) was applied to detect level of cell apoptosis. Glioma cells were collected after dissociation with trypsin without EDTA. Next, cells were washed by cold phosphate-buffered saline (PBS). Finally, cells were stained in the binding buffer with Annexin V-FITC and PI for an incubation of 15 min in the darkness. Cytoflex S (Beckman, USA) was utilized to check the staining ratio of FIFC/PI and calculate the level of apoptosis.

# Western blot

Total proteins were extracted using RIPA lysis buffer (1:1000) (Transgen, Beijing, China) and protease/phosphates inhibitors (APEBIO,USA). Concentration of proteins was measured by BCA Protein Quantification Kit (Vazyme, China) before Western blot. Proteins were separated by 10% or 12.5% SDS-PAGE gel electrophoresis, transferred to PVDF membranes and probed with primary antibodies. The membranes were subsequently probed with horseradish peroxidase-conjugated secondary antibodies. Later, an enhanced chemiluminescence detection system (Bio-rad, USA) was utilized for protein development. Anti-GAPDH antibody was used to monitor the loading amount. Antibody information was displayed in Supplementary table 4.

# RNA segmentation, RNA pulldown and mass spectrum(MS) assay

ARST was divided into 5 segments (Boshang, China). For RNA segmentation, the full-length transcript of ARST is 2116 bp in length; Δ1, Δ2, Δ3, Δ4 and Δ5 correspond to the 1–470 bp, 471–801 bp, 802–1145 bp, 1146–1477 bp and 1477–2116 bp sequence fragments of ARST. For plasmid extraction, OMEGA Endo-free plasmid mini kit II (D6950-01, Shanghai, China) was applied. For enzyme digestion, we used FastDigest XhoI (ThermoFisher, USA) and obtained agarose gel electrophoresis images by the software Quantity One. For DNA purification and transcription in vitro, we utilized TIANquick Mini Purification Kit (DP203) (Beijing, China) and MEGAscript T7 (Beijing, China). RNA pull-down assays were performed using a Pierce™ Magnetic RNA-Protein Pull-Down Kit (Thermofisher, USA) following the manufacturers' guideline. Biotinylated ARST was synthesized by Pierce™ RNA 3' End Desthiobiotinylation Kit (Thermofisher, USA). Mass spectrum (MS) was utilized to identify the proteins interacting with ARST and its segments.

# Peptide mutation and segmentation assay

For target protein mutation and segmentation, ALDOA was mutated on five sites separately: E35D, K42N/R43A, K149A, K294A (Boshang, China) according to the former studies [19, 20]. Considering the interaction between ALDOA and ARST according to the prognosis results on catRAPID website, ALDOA was also designed to be segmented into two parts (Boshang, China). ALDOA was cloned into the eukaryotic expression vector pcDNA3.1(+) with a C-terminal flag tag and translated to a 40kD protein. ALDOA lacking the 289–364 amino acid (AA) region was cloned into pcDNA3.1(+) to make the pcDNA3.1(+)-ALDOA-△1-flag construct, which could be translated to a 31.6 kDa protein; ALDOA lacking the 1–77 AA region was cloned into pcDNA3.1(+) to make the pcDNA3.1(+)-ALDOA-△2-flag construct, which could be translated to a 31.5 kDa protein.

# Protein co-immunoprecipitation (Co-IP) and RNA immunoprecipitation (RIP) assays

A RIP assay was performed using a specific RNA Immunoprecipition Kit (Geenseed, China) to detect the target RNAs and proteins according to the manufacturer's instructions. Firstly, whole-cell extracts prepared in lysis buffer containing a protease inhibitor cocktail and RNase inhibitor were incubated on ice for 40 min. Secondly, the former mixture was centrifuged at 13,000 g and 4 °C for 20 min and the supernatant was obtained. Magnetic beads were pre-incubated with 5 μg IP-grade antibodies for 30 min at room temperature with rotation about 10r/min. Thirdly, the supernatant was added to the bead-antibody complex in the immunoprecipitation buffer and incubated at 4 °C for 2 h. Later, liquid after overnight reaction was centrifuged in the specific spin columns. Finally, the spin columns were handled by RNase water and the dissolved RNA was purified and quantified by qRT-PCR. The proteins of each sample were precipitated with ice-cold acetone for Western blot examination.

# Lactic acid test assay

Cells were cultured in 96-well plate, 1000 cells per well. After 72 h, the cellular metabolism level was measured by Lactic Acid testing Kit (Jiancheng, Nanjing, China). Procedures were described previously [21]. Optical density value was measured at 530 nm on iMark Microplate Reader (Bio-Rad, USA).

# Enzymatic activities of PFK, PKM and HK

U87MG cells were seeded in six-well plates at a density of $2.0 \times 10^5$ per well, and cultured for 12 h before transfection. After transfection, cells were then digested by 0.08% EDTA trypsin after 48 h. The enzyme activities of PFK, PKM and HK were detected by the respective enzyme activity kit (Jiemei Genetech, Corporation, China) according to the manufacturer's instructions.

# Immunofluorescence and cytoskeleton co-staining

F-actin Staining Kit-Green Fluorescence-Cytopainter (Abcam) was applied for cytoskeleton co-staining with specific proteins. Cytoskeleton staining procedures were described previously [22]. For immunofluorescence, 24-well plates were selected to provide places for cell grow on the glass coverslips. After incubation with the antibodies overnight and AlexaFluor secondary antibodies for 1 h, the images were gained and handled on Zeiss LSM780 confocal laser scanning microscope system (Germany).

# Animal experiments

Aiming at the target lncRNA ARST, we designed lentivirus expression vector using human eukaryotic translation elongation factor 1 α1 promoter. GL261 cells, U87MG, C57 mice and BALB/c nude mice were chosen for experiments in vivo. C57 mice and BALB/c Nude immunodeficiency mice (5 weeks old) in the experiment were purchased from Beijing Weitong Lihua Experimental Technology Co., Ltd., and were housing in SPF (Specific pathogen free, SPF) class Animal Culture Center of Baotuquan Campus, Shandong University. Animal experiments were carried out obeying to the Guidelines of Laboratory Animals Using and Caring of Shandong University School of Qilu Medicine. Animal experimental procedures were acquired from the admissions of the Animal Care Committee of Shandong University. After lentivirus infection and puromycin selection, we set up the experimental cell line LV-EF1a > ARST-CMV > Luciferase/T2A/Puro, and the control cell line LV-CMV > Luciferase/T2A/Puro for animal

experiments (Cyagen, Guangzhou, China). Mice were anesthetized and the brains regions were stereotactically located, 2 mm away from skull midline of the right frontal, 2 mm behind the coronal suture. The located part was drilled and injected at a depth of 5 mm from the surface of the skull, with a speed of 0.2 μL per 15 s (Total injected cell number: $2.5 \times 10^6$). After the injection was completed, the needle was left for 2 min and then withdrawn 1 mm every minute. Animals were observed until neurological symptoms or signs appeared, including hunched posture, gait changes, lethargy and weight loss. After implantation for 7d and 14d, the animal imaging system IVIS Spectrum (PerkinElmer, USA) was applied for detecting the variation of the tumor size. For the rescuing experiments, BALB/c nude mice were applied for glioma cells implantation intracranially and after 21d, histologic section experiments were performed by the HE staining technique.

# Statistical analysis

GraphPad Prism software (La Jolla, CA, USA) was used for data analysis, and ImageJ (National Institutes of Health, USA) was used for figure analysis. T-test was used for comparing the statistical data of two groups. Chi-square test was used to analyze the correlation between the expressions of ARST and the glioma features. For qRT-PCR, the experimental systems were repeated three times independently. All data were displayed as mean ± standard error of mean (SEM). Moreover, P value < 0.05 was considered to be statistically significant.

## Results

# LncRNA ARST was significantly downregulated in the glioma samples

To identify novel lncRNAs involved in the development of gliomas, we carried out a lncRNA expression profile analysis using Affymetrix GeneChip® Human Transcriptome Array 2.0. NONHSAT138818.2, which we named lncRNA ARST (ALDOA related specific transcript) exhibited significant downregulation in the glioma tissues compared to the paracarcinomic and normal tissues (Fig. 1A). Then we used NCBI ORFinder online tool (https://www.ncbi.nlm.nih.gov/orffinder/) to detect the number of ORFs in the RNA sequence. The results showed that 23 sense ORFs with potential to encode peptides were included. However, these 23 peptides indicated no significantly similar proteins or peptides when they were compared in the swiss-prot database using the NCBI BLAST tool (Supplementary table 1). Additionally, the PhyloCSF value of ARST, which was calculated to verify the conservation of the sequence, was minus. In conclusion, we identified that ARST could not encode protein and it was a long non-coding RNA [23, 24] (Fig. 1B).

We subsequently analyzed the expression levels of ARST in more glioma and corresponding non-cancerous tissues using qRT-PCR analysis. The results showed that the expressions of ARST were significantly downregulated in the glioblastoma multiform (GBM) tissues compared to the low grade glioma (LGG) and non-cancerous tissues (Fig. 1C). Furthermore, ARST levels were negatively correlated

with the pathological grades of the gliomas. (Fig. 1D). In the gliomablastoma cell lines U87MG and U251, ARST was conceivably lower in comparative to normal human astrocytes (Fig. 1E), further suggesting the potential role of ARST in gliomagenesis.

According to the NONCODE database, ARST is one of the transcripts derived from LINC00632, which mainly distributes in the human brain based on the GEPIA database (Supplementary Fig. 1A). Compared with normal tissues, the expressions of LINC00632 were significantly downregulated in both tissues of GBM and LGG (Supplementary Fig. 1B-1D). Moreover, low LINC00632 expression correlated with poor overall survival and disease-free survival in the glioma patients (Supplementary Fig. 1E, 1F). Fluorescence in situ hybridization (FISH) assay was further utilized to examine the distribution of ARST in the U87MG cells. The results showed that ARST mainly located in the cytoplasm of the cells (Fig. 1F). The U251 cell line displayed a similar result (Supplementary Fig. 1G).

# ARST inhibited the malignant phenotypes of glioma cells

To elucidate the functions of ARST in gliomas, we transfected both the U87MG and U251 glioma cells with the plasmids expressing ARST (oeARST) or ARST Smart Silencer (siARST). Nonspecific vectors were used as the negative control. qRT-PCR analysis indicated an increase by approximately 15 times in the oeARST-transfected cells compared with the control (Fig. 2A). However, siARST only resulted in a modest decrease of ARST in these cells (Supplementary Fig. 2A, 2B).

A traditional CCK-8 assay was performed to evaluate whether ARST would affect viability of the glioma cells. As the results shown in Fig. 2B, cell growth was markedly inhibited in both of the U87MG and U251 cells when ARST was increased (Fig. 2B). However, the change in cell growth caused by knocking down ARST was not significant (Supplementary Fig. 2C, 2D). To further clarify whether reduction of cell viability in the ARST upregulated cells resulted from changes in cell proliferation or apoptosis, EdU cell proliferation assay was applied. As depicted in Fig. 2C, number of EdU positive cells was significantly decreased when ARST was overexpressed in both cell lines (Fig. 2C). What's more, duel-staining with Annexin V and PI followed by flow cytometry assay indicated that 17.36% of U87MG and 11.87% of U251 cells underwent apoptosis with upregulation of ARST; while only 7.96% and 6.13% of apoptotic cells were observed in the cells transfected with the negative control (Fig. 2D).

As one of the most aggressive malignant brain tumors, gliomas are characterized with massive infiltrative growth without boundary from surrounding tissues [25]. Therefore, to investigate whether ARST contributes to the migration and invasion of glioma cells, transwell and wound-healing assays were performed. The results showed that number of the migrating or invading cells with ARST overexpression was decreased compared to that of the control cells, with average reduction rate of 34.5% for the U87MG cells and 39.9% for the U251 cells, respectively (Fig. 2E). On the othe hand, repair of scratches was significantly suppressed when ARST was upregulated in the both cells line after 12 hours of incubation (Fig. 2F) [26].

Considering the in vitro involvement of ARST in glioma cell proliferation, migration and invasion, we extended this study to determine the impact of ARST on tumorigenic capabilities of gliomas in vivo. When the GL261 cells transduced with lentiviral vectors expressing ARST or negative control plasmids were intracranially implanted into the C57 mice, we observed a significant decrease in tumor formation in the tumor-bearing mice when ARST was overexpressed (Fig. 2G). Furthermore, these mice achieved longer survival in comparison to the control mice (Fig. 2H).

# ARST interacted with ALDOA to exert its functions in glioma development

In order to identify the proteins that interact with ARST, biotin-labeled RNA pulldown followed by a mass spectrometry-based assay was conducted (Fig. 3A). The results revealed that 125 proteins were differentially bound to the sense and anti-sense strands of ARST in the U87MG cells (Supplementary table 2). Based on the score of peptide identification, we discovered that ALDOA was one of the highly enriched proteins (Fig. 3B), which was further verified by Western blot (Fig. 3C). Moreover, in the silver staining assay, coinciding with the position of ALDOA, a 40 kDa band showed up in the protein lysate that bound to the sense strand of ARST, while it was missing in the lysate that bound to the anti-sense strand of ARST (Supplementary Fig. 3A). To further validate the physical interaction between ARST and ALDOA, we subsequently performed a RIP assay with an anti-ALDOA antibody and found that ARST was obviously enriched (Fig. 3D), evidently confirming the above results.

To determine the specific fragments of ARST required for its interaction with ALDOA, we constructed a series of ARST truncation plasmids according to the loop structures of ARST transcript (Fig. 3E) and conducted RNA pulldown assay. The results indicated that the 1146-1477nt (Δ4) and 1478-2116nt (Δ5) regions of ARST potentially mediated its interaction with ALDOA (Fig. 3F). However, upregulation of ARST affected neither the protein or mRNA levels of ALDOA (Fig. 3G, 3H). These results suggested that ARST might exert its functions via binding to ALDOA, instead of regulating the expression of ALDOA.

We subsequently examined the transcriptional and survival data of ALDOA in patients with LGG and GBM from the GEPIA database. The results showed that there was no significant difference in the expression levels of ALDOA between the LGG/GBM and normal brain tissues (Fig. 3I). However, The overall and disease-free survivals of the glioma patients with high-level of ALDOA were obviously lower than that with low level of expression (Fig. 3J, 3K). Then we took a step further to explore the correlation of LINC00632 and ALDOA via log2 FPKM. The Pearson's correlation co-efficiency of LINC00632 and ALDOA was − 0.15 (Fig. 3L), which might further indicate that the relationship between ARST and ALDOA did not occur on the level of transcription.

# ARST regulated ALDOA mediated actin filament integrity instead of its enzymatic activity

We analyzed the proteins obtained in the RNA pulldown by mass spectrometry. The proteins that only bound to the sense strand of ARST were used to construct a PPI (Protein-protein interaction) network

using the STRING database (www.string.org) (Supplementary Fig. 3B). At the same time, these proteins were enriched by the Metascape database (www.metascape.org) and clustered using its built-in MCODE algorithm (Fig. 4A, 4B). We found that the pathways in which ALDOA was closely involved were tumor metabolism and smooth muscle contraction. According to the description of smooth muscle contraction in the Reactome database (https://reactome.org), this pathway mainly includes cytoskeleton related protein components such as actin, myosin and intermediate filaments. As previously reported, this refers to the non-enzymatic or moonlight effect of ALDOA.

To determine whether ARST regulated the enzymatic activity of ARST, the concentration of lactic acid in the culture medium of the U87MG cells was examined. As the results shown in Fig. 4C, no significant fluctuation appeared in the lactate levels when ARST was overexpressed (Fig. 4C). Furthermore, the activities of the key enzymes involved in glycolysis had hardly changed in these cells (Fig. 4D).

On the other hand, we noticed an obvious morphological change in the ARST upregulated cells which exhibited less dentrite-like structures in comparison to the control cells. Furthermore, immunofluorescence with phalloidin staining indicated that actin stress fibers were intact in the control cells, however, they almost disappeared in the cells with ARST overexpression (Fig. 4E). In order to clarify the relationship between ALDOA and F-actin, dual staining with the antibody to recognize ALDOA as well as phalloidin was performed. The result showed that in the control cells, ALDOA exhibited a significant enrichment on the actin filaments. In contrast, with the disappearance of actin fibers, ALDOA were diffusely distributed in the ARST upregulated cells (Fig. 4F). This phenomenon evidently suggested that ARST might regulate the role of ALDOA in actin fiber integrity instead of its enzymatic activity.

# ARST decreased the interactions of ALDOA, cofilin and F-actin, respectively

Considering the negative role of ARST in ALDOA mediated actin fiber integrity, we made a step further to explore whether other proteins were involved in the depolymerization of actin filaments when ARST was overexpressed. Based on the PDB database and previous literature [27], we found that cofilin, an actin depolymerizing protein (ADP) took effects in interacting with F-actin and further depolymerizing it.

A subsequent separation from cofilin leads to the release of G-actin monomers, which would be further used to promote the assembly of new F-actin fiber [14]. Most interestingly, it was reported, given the large globular shapes of ALDOA and cofilin, they shared an extensive overlap binding sites on F-actin [11, 27, 28]. It was therefore proposed that ARST detached ALDOA from F-actin. The exposed binding sites were further bound by cofilin which led to the depolymerization of actin filaments.

To prove the above hypothesis, co-immunoprecipitation was performed to detect the interactions between ALDOA, cofilin and F-actin. The results demonstrated that upregulation of ARST significantly decreased the binding capacity of ALDOA to F-actin (Fig. 5A). The interactions between cofilin and F-actin were reduced as well, compared to the negative control (Fig. 5B). Immunofluorescence of cofilin as well as phalloidin was further conducted. The result showed that in the control cells, cofilin localized with

obvious dotted structures on the actin stress fibers. Overexpression of ARST led to obvious disappearance of F-actin. The distributions of cofilin and depolymerized actin were separated in the cytoplasm, which was consistent with the co-immunoprecipitation results (Fig. 5C). This phenomenon evidently suggested that cofilin was involved in the depolymerization of actin stress fibers following the detachment of ALDOA from F-actin by upregulation of ARST.

We subsequently examined the transcriptional and survival data of cofilin in the patients with LGG and GBM from the GEPIA database. The results showed that the expressions of cofilin were significantly upregulated in the LGG/GBM samples compared to the normal brain tissues (Fig. 5D). Consistently, the overall and disease-free survivals of the glioma patients with high-levels of cofilin were lower than that with low level expressions of cofilin (Fig. 5E, 5F).

# ARST interacted with the binding sites of ALDOA and F-actin

In order to investigate the detailed mechanisms involved in ARST mediated separation of ALDOA from F-actin, CatRAPID database (http://service.tartaglialab.com/page/ catrapid_group) was utilized to predict the binding sites of ARST on ALDOA. The results demonstrated that ARST potentially bound to the 289–340 amino acids of ALDOA (Fig. 6A, 6B). On the other hand, ALDOA potentially interacted with the 1276-1361nt of ARST, which was consistent with the previous result in Fig. 3F (Supplementary Fig. 4A). To verify the specific regions of ALDOA required for its binding with ARST, we constructed ALDOA truncation plasmids including or excluding the prognostic domains based on the catRAPID database and conducted RNA pulldown assay (Supplementary table 3). The results indicated that the 289–364 amino acids of ALDOA was indeed required for its interaction with ARST (Fig. 6C, 6D).

What's more, it was previously reported that the amino acids E35, K42, R43, K149, K294 of ALDOA contributed to the interaction between ALDOA and actin filaments [15, 20]. To verify whether ARST affected any of the above amino acids, we constructed a series of ALDOA plasmids with the mutated amino acids E35D, K42N/R43A, K149A and K294A respectively (Fig. 6E; Supplementary Fig. 4B-4E). The subsequent RNA pulldown assay indicated that K294 was essential for the interaction between ARST and ALDOA (Fig. 6F). It was thus hypothized that ARST might bind to K294 of ALDOA, which in turn weakened the interaction of ALDOA with F-actin.

# Upregulation of ALDOA alleviated the inhibitory effects of ARST in gliomas

Given that ARST suppressed gliomagenesis and that ALDOA was a potential target of ARST, we next investigated whether ALDOA represented a functional link for the biological changes observed in the glioma cells with ARST upregulation. To confirm this hypothesis, U87MG and U251 cell lines were first transfected with the plasmids overexpressing ARST, which were termed oeARST cells. Furthermore, we transfected these oeARST cells with the plasmids designated to ALDOA to investigate the responses to ALDOA upregulation. As expected, the efficiency of ARST in inhibiting cell invasion, migration (Fig. 7A, 7B) and proliferation (Fig. 7C) were significantly alleviated when ALDOA was induced. Moreover,

upregulation of ALDOA significantly restored the actin stress fibers in the oeARST cells (Fig. 7D). The nude mice which were intracranially transplanted the ARST/ALDOA double upregulated cells exhibited larger tumor size and poorer prognosis compared to that transplanted with oeARST cells (Fig. 7E). Taken together, all these data suggested that the tumor suppressive role of ARST in gliomagenesis might be largely dependent on ALDOA.

# Discussion

Glioma is one of the most common malignant tumors in the central nervous system. It is characterized with rapid progression, poor prognosis and high recurrence rate. Due to the strong infiltrative ability to the surrounding tissues, the recurrence rate of the glioma is almost 100%, making it extremely difficult for neurosurgeons to deal with it effectively [29].

Cytoskeleton plays an essential role in the motion dynamics of the cells [30], one of the most important component of which is fibrous actin (F-actin). Marie France Carlier et al. reported that actin filaments were depolymerized by cofilin, a kind of actin depolymerization protein (ADP) [14]. It was conducive to the fracture of the old actin fibers and accelerated the formation of new F-actin. Yu Chan Chang et al., on the other hand, elaborated the important role of ALDOA in the polymerization and stabilization of actin filaments [15]. Therefore, under normal circumstances, the polymerization and depolymerization of F-actin exist together, which maintains a dynamic balance to ensure the normal movement, morphological changes and other life activities of the cells.

Recently in 2019, Agnieszka gizak et al. found that ALDOA and cofilin had overlapping binding sites on F-actin [11]. Among them, ALDOA, which was indispensable for actin fiber reorganization, had a stronger capacity to bind F-actin, so that the actin cytoskeleton was kept in a stable state in most cases. Compared with the cells in normal tissues, ALDOA and cofilin were often overexpressed in the cells of various tumors. Especially in the glioma cells, which exhibited a strong invasive ability, cofilin was significantly upregulated [31, 32]. High level of cofilin led to the enhanced depolymerization and re-polymerization of actin fibers which promoted malignant invasion and migration of gliomas [33]. Furthermore, it was also reported that both ALDOA and cofilin could be used as promising indicators for glioma radio-sensibility and prognosis [34].

Up to now, researches in tumor development have focused mostly on protein-coding genes. However, the functions and contributions of non-coding RNAs remain insufficiently defined [35]. Based on a large-scale microarray profiling, we identified a novel long non-coding RNA, ALDOA Related Specific Transcript (ARST) which was significantly suppressed in the glioma tissues. It contains 2116 nucleotides and has never been recorded in the Ensemble database. In contrast, we found the information of the parental transcript of ARST, LINC00632. According to the TCGA database, LINC00632 is downregulated in the glioma tissues and glioma cell lines. The glioma patients with high expression level of LINC00632 are associated with better long-term and disease-free survivals, potentially suggesting a similar role of ARST in gliomagenesis.

To verify the assumption, we overexpressed ARST in the glioma cell lines. The results showed that ARST inhibited the malignant phenotypes of the glioma cells such as viability, proliferaition, invasion, migration and xenograph tumor growth. However, the level of lactic acid and activities of the key enzymes involved in glycolysis had hardly changed, suggesting a non-metabolic role of ARST in these cells. We further identified that ARST interacted with the crucial domain of ALDOA through which ALDOA binds to F-actin. Overexpression of ARST decreased the binding capacities of ALDOA to F-actin, leading to the severe disintegration of actin fibers. The interaction between cofilin and actin was affected as well.

It is thus hypothized that in normal cells, the polymerization and depolymerization of F-actin are orderly and strictly controlled, among which ARST plays a negative regulatory role in occupying ALDOA so that the excessive formation of F-actin is avoided. However, in the glioma cells, down-regulation of ARST deceases its restraint on ALDOA. Simultaneous induced expression of cofilin accelerates the speed of depolymerization of old F-actin and re-polymerization of new actin fibres. That probably explains the significant infiltrative property of gliomas. When we overexpressed ARST in the glioma cells, it interrupted the interaction of ALDOA and actin filaments, so that more binding sites of F-actin were exposed to cofilin, which in turn led to the depolymerization of actin cytoskeleton. On the other hand, without the interaction of ALDOA, formation of new actin fibers were significantly inhibited (Fig. 8).

Taken together, it is concluded that ARST performs its function via regulating the dynamic equilibrium and integrity of actin cytoskeleton through ALDOA and cofilin, which in turn modifies the morphology and invasive properties of the glioma cells. This has added new perspective to its role in tumorigenesis, thus providing potential therapeutic targets for glioma treatment.

# Conclusions

In this study, we reported that a novel lncRNA ARST was downregulated in the gliomas. Overexpression of ARST in the glioma cells significantly suppressed cell viability, proliferation, invasion and migration in addition to an increase in apoptosis. The tumorigenic capacity of these cells in vivo was reduced as well. We further demonstrated that the tumor suppressive effects of ARST could be mediated by a direct binding to ALDOA, which together with cofilin, maintains an orderly and strictly controlled balance of polymerization and depolymerization of actin filaments. Upregulation of ARST interrupted the interaction of ALDOA and actin fibers, so that more binding sites of F-actin were exposed to cofilin, which in turn led to the depolymerization of actin cytoskeleton. On the other hand, without the interaction of ALDOA, formation of new actin fibers was significantly inhibited.

ARST performed its function via regulating the dynamic equilibrium and integrity of actin cytoskeleton through ALDOA and cofilin, which in turn modified the morphology and invasive property of the glioma cells. This has added a new perspective to its role in tumorigenesis, thus providing potential target for glioma diagnosis, therapy, and prognosis.

# Abbreviations

ARST
ALDOA-related specific transcript NONSHAT138818.2;ALDOA:aldolase A; GBM:glioblastoma multiforme; LGG:low-grade glioma; FBS:fetal bovine serum; DMEM:dulbecco's modified eagle medium; qRT-PCR:quantitative real-time PCR; EdU:5-ethynyl-2’-deoxyuridine; DAPI:4’,6-diami-dino-2-phenylindole; BCA:bicinchoninic acid; co-IP:co-immunoprecipitation; IF:immunofluorescence; NHA:normal human astrocytes; ADP:actin depolymerizing protein

# Declarations

### Availability of data and materials

The datasets during and/or analyzed during the current study are available from the corresponding author on reasonable request.


### Grant support

We thank Translational Medicine Core Facility of Shandong University for consultation and instrument availability that support this work. This work was supported by grants from Natural Science Foundation of China: Grant No. 81771270, No.81871196, No.81471517. Shandong Provincial Natural Science Foundation, China: Grant No. ZR2018MH005. Shandong Province Key Research and Development Program: Grant No. 2019GSF107046, No.2019GSF108250.


### Authors’ contributions

Qian Liu, Qi Pang, Dong He and Jun Sun generated the hypothesis and designed the experiments. Jun Sun, Taihong Gao, Yanan Wang and Hua Guo performed experiments. Dong He, Rui Zhang and Yanbang Wei performed the animal experiments. Dong He, Yibing Fu and Jun Sun interpreted the data. Qian Liu, Yuji Guo, Zhaojuan Wang and Jun Sun wrote the manuscript. Qian Liu and Qi Pang supervised the overall research, secured funding, and interpreted results.

### Ethics approval

This study was reviewed and approved by the Ethical Board at Shandong Provincial Hospital, Cheeloo College of Medicine, Shandong University.

### Consent for publication

All authors agreed on the manuscript.

### Competing interests

The authors declare no conflict of interests.

# References

1. Chen H, Huang Q, Dong J, Zhai DZ, Wang AD, Lan Q. Overexpression of CDC2/CyclinB1 in gliomas, and CDC2 depletion inhibits proliferation of human glioma cells in vitro and in vivo. Bmc Cancer. 2008; 10.1186/1471-2407-8-29
2. Yi DA, Hua TX, Lin HY. EGFR Gene Overexpression Retained in an Invasive Xenograft Model by Solid Orthotopic Transplantation of Human Glioblastoma Multiforme Into Nude Mice. Cancer Investigation. 2011; 10.3109/07357907.2010.550665
3. Salyakina D, Tsinoremas NF. Non-coding RNAs profiling in head and neck cancers. Npj Genomic Medicine. 2016; 10.1038/Npjgenmed.2015.4
4. Rani N, Nowakowski TJ, Zhou HJ, Godshalk SE, Lisi V, Kriegstein AR, Kosik KS. A Primate lncRNA Mediates Notch Signaling during Neuronal Development by Sequestering miRNA. Neuron. 2016; 10.1016/j.neuron.2016.05.005
5. Xu YJ, Wu W, Han Q, Wang YL, Li CC, Zhang PP, Xu HX. New Insights into the Interplay between Non-Coding RNAs and RNA-Binding Protein HnRNPK in Regulating Cellular Functions. Cells-Basel. 2019; Artn 62 10.3390/Cells8010062
6. Han MZ, Wang S, Fritah S, Wang X, Zhou WJ, Yang N, Ni SL, Huang B, Chen AJ, Li G, Miletic H, Thorsen F, Bjerkvig R, Li XG, Wang J. Interfering with long non-coding RNA MIR22HG processing inhibits glioblastoma progression through suppression of Wnt/beta-catenin signalling. Brain. 2020; 10.1093/brain/awz406
7. Tan SK, Pastori C, Penas C, Komotar RJ, Ivan ME, Wahlestedt C, Ayad NG. A Primate lncRNA Mediates Notch Signaling during Neuronal Development by Sequestering miRNA. Mol Cancer. 2016; 10.1016/j.neuron.2016.05.005
8. Li X, Jiang FX, Ge Z, Chen B, Yu J, Xin MJ, Wang JD, An LX, Wei JC, Wu LQ. Fructose-Bisphosphate Aldolase A Regulates Hypoxic Adaptation in Hepatocellular Carcinoma and Involved with Tumor Malignancy. Digest Dis Sci. 2019; 10.1007/s10620-019-05642-2
9. Na N, Li H, Xu CF, Miao B, Hong LQ, Huang ZY, Jiang Q. High expression of Aldolase A predicts poor survival in patients with clear-cell renal cell carcinoma. Ther Clin Risk Manag. 2017; 10.2147/Tcrm.S123199
10. Du S, Guan ZZ, Hao LH, Song Y, Wang L, Gong LL, Liu L, Qi XY, Hou ZY, Shao SJ. Fructose-Bisphosphate Aldolase A Is a Potential Metastasis-Associated Marker of Lung Squamous Cell Carcinoma and Promotes Lung Cell Tumorigenesis and Migration. Plos One. 2014; ARTN e85804 10.1371/journal.pone.0085804
11. Gizak A, Wisniewski J, Heron P, Mamczur P, Sygusch J, Rakus D. Targeting a moonlighting function of aldolase induces apoptosis in cancer cells. Cell Death Dis. 2019; Artn 712 10.1038/S41419-019-1968-4
12. Tokuraku K, Kuragano M, Uyeda TQP. Long-Range and Directional Allostery of Actin Filaments Plays Important Roles in Various Cellular Activities. Int J Mol Sci. 2020; Artn 3209 10.3390/Ijms21093209
13. Wang Q, Crevenna AH, Kunze I, Mizuno N. Structural basis for the extended CAP-Gly domains of p150(glued) binding to microtubules and the implication for tubulin dynamics. P Natl Acad Sci USA.

2014; 10.1073/pnas.1403135111

14. Carlier MF, Ressad F, Pantaloni D. Control of actin dynamics in cell motility - Role of ADF/cofilin. J Biol Chem. 1999; DOI 10.1074/jbc.274.48.33827
15. Chang YC, Chiou J, Yang YF, Su CY, Lin YF, Yang CN, Lu PJ, Huang MS, Yang CJ, Hsiao M. Therapeutic Targeting of Aldolase A Interactions Inhibits Lung Cancer Metastasis and Prolongs Survival. Cancer Res. 2019; 10.1158/0008-5472.CAN-18-4080
16. Xu WG, Zhou B, Wu J, Jiang P, Chen HQ, Yan F. Circular RNA hsa-circ-0007766 modulates the progression of Gastric Carcinoma via miR-1233-3p/GDF15 axis. Int J Med Sci. 2020; 10.7150/ijms.46261
17. Cheng Q, Zeng KR, Kang QY, Qian WT, Zhang WY, Gan QL, Xia WW. The Antimicrobial Peptide LL-37 Promotes Migration and Odonto/Osteogenic Differentiation of Stem Cells from the Apical Papilla through the AktANnt/beta-catenin Signaling Pathway. J Endodont. 2020; 10.1016/j.joen.2020.03.013
18. Ji H, Hui BQ, Wang JR, Zhu Y, Tang LY, Peng P, Wang TJ, Wang LJ, Xu SF, Li J, Wang KM. Long noncoding RNA MAPKAPK5-AS1 promotes colorectal cancer proliferation by partly silencing p21 expression. Cancer Sci. 2019; 10.1111/cas.13838
19. Peng W, Zhang C, Peng JN, Huang YJ, Peng CF, Tan YQ, Ji DJ, Zhang Y, Zhang DS, Tang JW, Feng YF, Sun YM. Lnc-FAM84B-4 acts as an oncogenic lncRNA by interacting with protein hnRNPK to restrain MAPK phosphatases-DUSP1 expression. Cancer Lett. 2020; 10.1016/j.canlet.2020.08.036
20. Kusakabe T, Motoki K, Hori K. Mode of interactions of human aldolase isozymes with cytoskeletons. Arch Biochem Biophys. 1997; DOI 10.1006/abbi.1997.0204
21. Li J, Liu Q, Liu ZH, Xia Q, Zhang ZH, Zhang R, Gao TH, Gu GY, Wang YA, Wang D, Chen XY, Yang YH, He D, Xin T. KPNA2 promotes metabolic reprogramming in glioblastomas by regulation of c-myc. J Exp Clin Canc Res. 2018; Artn 194 10.1186/S13046-018-0861-9
22. Song Y, Wu KY, Wu WJ, Duan ZY, Gao YF, Zhang LD, Chong T, Garstka MA, Zhou WD, Li K. Epithelial C5aR1 Signaling Enhances Uropathogenic Escherichia coil Adhesion to Human Renal Tubular Epithelial Cells. Front Immunol. 2018; Artn 949 10.3389/Fimmu.2018.00949
23. Lin MF, Jungreis I, Kellis M. PhyloCSF: a comparative genomics method to distinguish protein coding and non-coding regions. Bioinformatics. 2011; 10.1093/bioinformatics/btr209
24. Mudge JM, Jungreis I, Hunt T, Gonzalez JM, Wright JC, Kay M, Davidson C, Fitzgerald S, Seal R, Tweedie S, He L, Waterhouse RM, Li Y, Bruford E, Choudhary JS, Frankish A, Kellis M. Discovery of high-confidence human protein-coding genes and exons by whole-genome PhyloCSF helps elucidate 118 GWAS loci. Genome Res. 2019; 10.1101/gr.246462.118
25. Bie L, Zhao G, Wang YP, Zhang B. Kinesin family member 2C (KIF2C/MCAK) is a novel marker for prognosis in human gliomas. Clin Neurol Neurosur. 2012; 10.1016/j.clineuro.2011.11.005
26. Yang P, Li J, Peng CF, Tan YQ, Chen RR, Peng W, Gu Q, Zhou JH, Wang L, Tang JW, Feng YF, Sun YM. TCONS_00012883 promotes proliferation and metastasis via DDX3/YY1/MMP1/PI3K-AKT axis in colorectal cancer. Clin Transl Med. 2020; ARTN e211 10.1002/ctm2.211

27. Tanaka K, Takeda S, Mitsuoka K, Oda T, Kimura-Sakiyama C, Maeda Y, Narita A. Structural basis for cofilin binding and actin filament disassembly. Nat Commun. 2018; Artn 1860 10.1038/S41467-018-04290-W
28. Hu GQ, Taylor DW, Liu J, Taylor KA. Identification of interfaces involved in weak interactions with application to F-actin-aldolase rafts. J Struct Biol. 2018; 10.1016/j.jsb.2017.11.005
29. Chung T, Na J, Kim YI, Chang DY, Kim YI, Kim H, Moon HE, Kang KW, Lee DS, Chung JK, Kim SS, Suh-Kim H, Paek SH, Youn H. Dihydropyrimidine Dehydrogenase Is a Prognostic Marker for Mesenchymal Stem Cell-Mediated Cytosine Deaminase Gene and 5-Fluorocytosine Prodrug Therapy for the Treatment of Recurrent Gliomas. Theranostics. 2016; 10.7150/thno.14158
30. Islam SMA, Patel R, Bommareddy RR, Khalid KM, Acevedo-Duncan M. The modulation of actin dynamics via atypical Protein Kinase-C activated Cofilin regulates metastasis of colorectal cancer cells. Cell Adhes Migr.2019; 10.1080/19336918.2018.1546513
31. Dettling S, Stamova S, Warta R, Schnolzer M, Rapp C, Rathinasamy A, Reuss D, Pocha K, Roesch S, Jungk C, Warnken U, Eckstein V, Grabe N, Schramm C, Weigand MA, von Deimling A, Unterberg A, Beckhove P, Herold-Mende C. Identification of CRKII, CFL1, CNTN1, NME2, and TKT as Novel and Frequent T-Cell Targets in Human IDH-Mutant Glioma. Clin Cancer Res. 2018; 10.1158/1078-0432.CCR-17-1839
32. Sun WB, Yan H, Qian CF, Wang CH, Zhao MJ, Liu YC, Zhong YJ, Liu HY, Xiao H. Cofilin-1 and phosphoglycerate kinase 1 as promising indicators for glioma radiosensibility and prognosis. Oncotarget. 2017; 10.18632/oncotarget.19025
33. Zhuang H, Li Q, Zhang XR, Ma XD, Wang Z, Liu Y, Yi XF, Chen RB, Han F, Zhang N, Li YM. Downregulation of glycine decarboxylase enhanced cofilin-mediated migration in hepatocellular carcinoma cells. Free Radical Bio Med. 2018; 10.1016/j.freeradbiomed.2018.03.003
34. Yan H, Yang K, Xiao H, Zou YJ, Zhang WB, Liu HY. Over-Expression of Cofilin-1 and Phosphoglycerate Kinase 1 in Astrocytomas Involved in Pathogenesis of Radioresistance. Cns Neurosci Ther. 2012; 10.1111/j.1755-5949.2012.00353.x
35. Gao TH, Gu GY, Tian JX, Zhang R, Zheng XR, Wang YA, Pang Q, Liu Q. LncRNA HSP90AA1-IT1 promotes gliomas by targeting miR-8855p-CDK2 pathway. Oncotarget. 2017; 10.18632/oncotarget.20777

# Figures

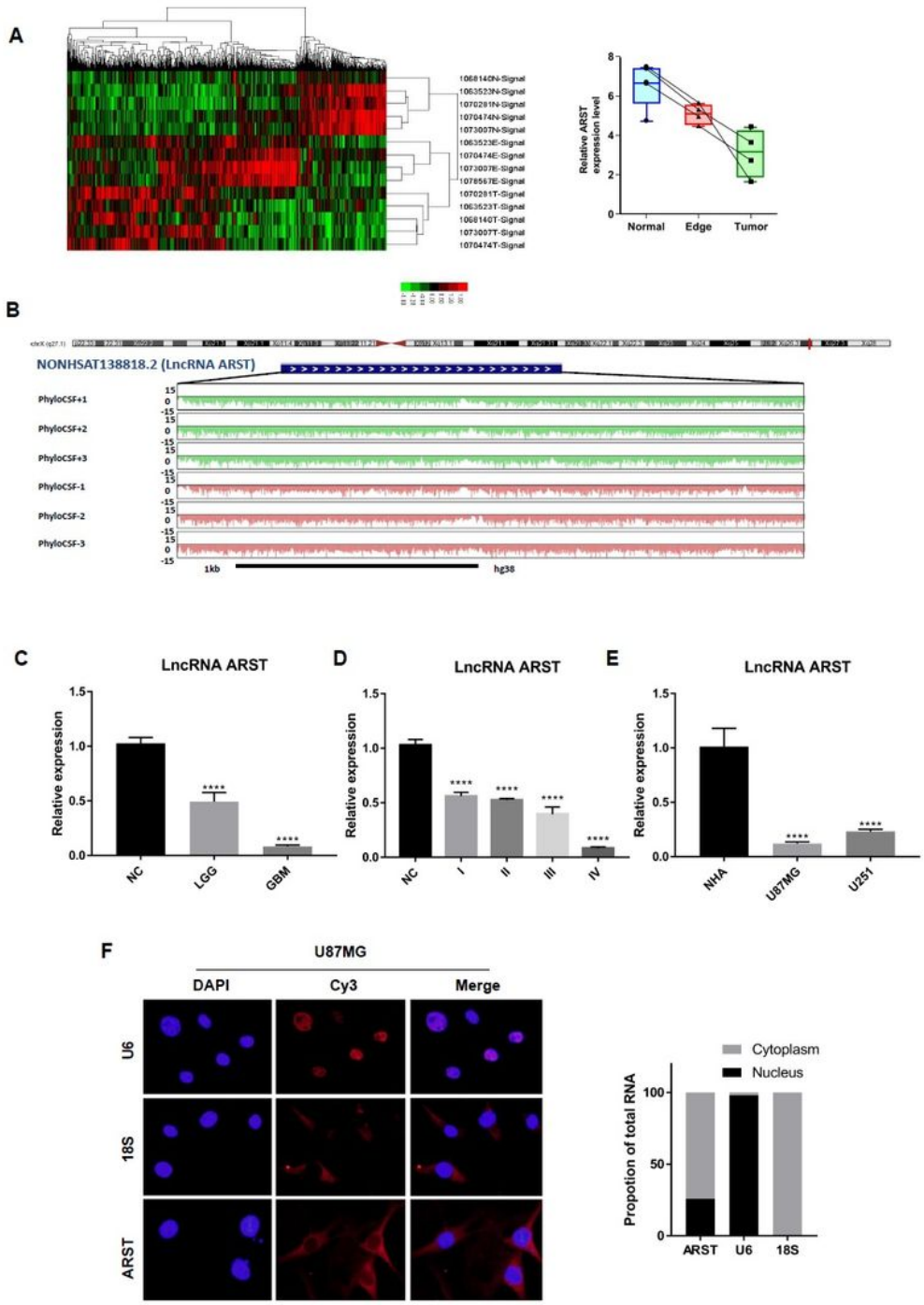


## Figure 1

LncRNA ARST was significantly downregulated in the gliomas (A) The differential expression clusters of lncRNAs in the glioma specimens and paracarcinomic tissues were shown. The suffix E-Signal represented edge tissues, the suffix T-Signal represented tumor tissues and the suffix N-Signal represented normal tissues. The red color indicated the upregulated lncRNAs and the green color indicated the downregulated lncRNAs (left). The expression levels of ARST in the different tissues were

displayed (right). Data are presented as mean ± s.d. from three independent experiments. (B) LncRNA location and PhyloCSF value analysis were shown by UCSC genome browser with PhyloCSF data hub. NCBI ORFinders online tool and PhyloCSF values of ARST were used to verify the conservation of the sequence. The differential expression levels of ARST in the clinical glioma specimens classified into low grade glioma (LGG), glioblastoma (GBM) tissues (C) or four World Health Organization (WHO) grades (D) were examined using qRT-PCR. The results are presented as mean ± s.d. from three independent experiments. (E) The expressions of ARST in the two glioma cell lines were tested by qRT-PCR compared to normal astrocytes (NHA). Each bar represents mean ± s.d. from three independent experiments. (F) Fluorescence in situ hybridization (FISH) assay was performed to detect the location of ARST in the U87 cells. Human 18S was used as a cytoplasm internal control and human U6 was used as a nucleus internal control (left). Propotions of ARST and the internal controls were determined in the cytoplasm and nucleus of the cells (right). ****P < 0.001.

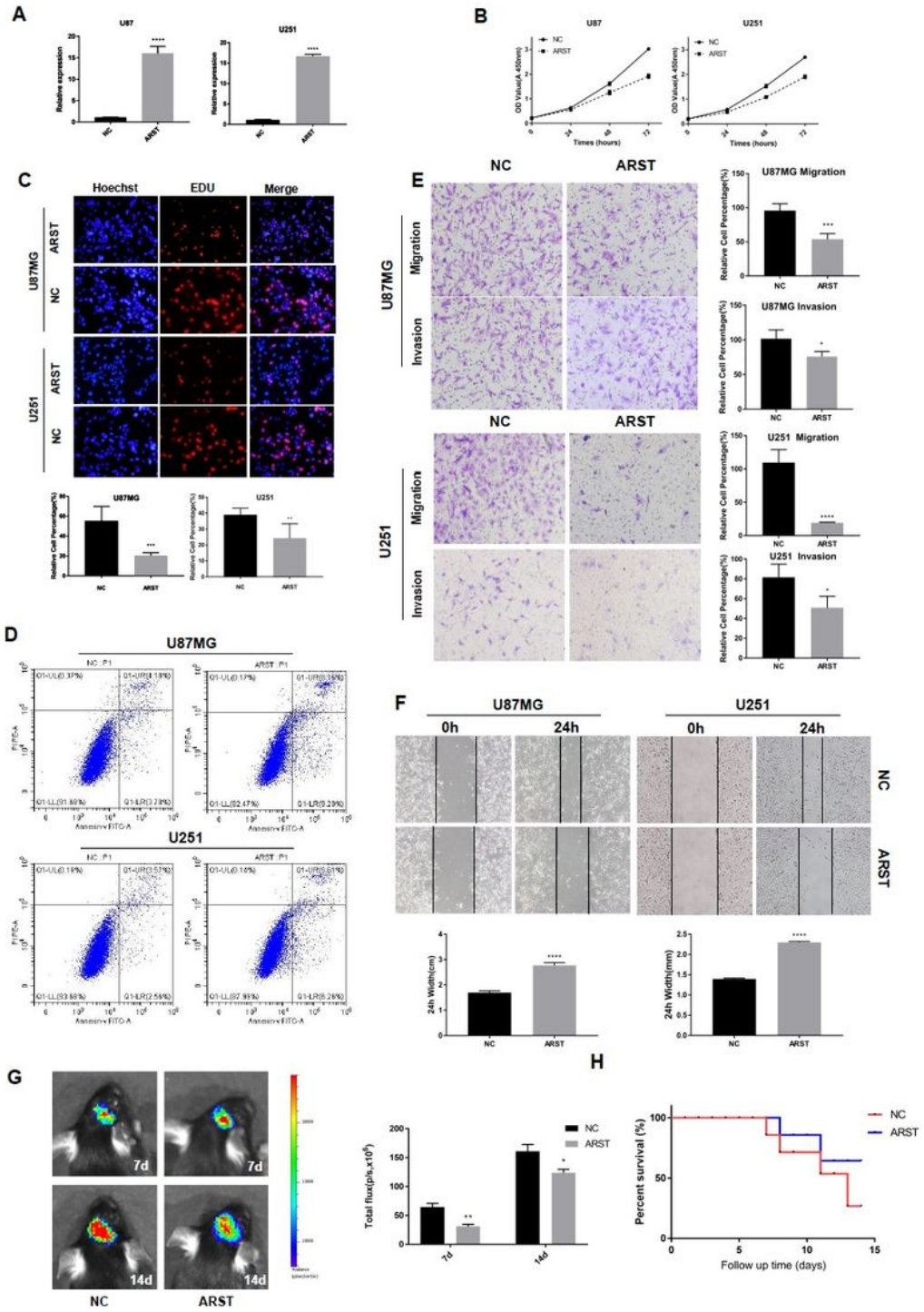


## Figure 2

ARST inhibited the malignant phenotypes of the glioma cells (A) The efficiencies of ARST overexpression in the U87MG and U251 cells were tested by qRT-PCR. Each bar represents mean ± s.d. from three independent experiments. (B) The growth curves of the transfected glioma cells were shown using CCK-8 assay. The results are presented as mean ± s.d. from three independent experiments. (C) An EdU staining assay was performed to determine the proliferation of the transfected U87MG and U251 cells. Data are

presented as mean ± s.d. from three independent experiments. (D) Apoptosis of the transfected cells were analyzed by duel staining of Annexin V and PI followed by flow cytometry assay. (E) Migration and invasion of the transfected cells were determined by transwell assay. Each bar represents mean ± s.d. from three independent experiments. (F) Wound-healing assay was performed. The data are presented as mean ± s.d. from three independent experiments. (G) Representative images and total flux of the C57 mice 7 days and 14 days after intracranial implantation of the GL261 cells transfected with luminance tagged ARST or control plasmids by IVIS spectrum. Each bar represents mean ± s.d. from three independent experiments. (H) Surviving curves of the C57 mice with xenographed tumors intracranially was recorded for 15 days. *P < 0.05, **P < 0.01, ***P < 0.005, ****P < 0.001.

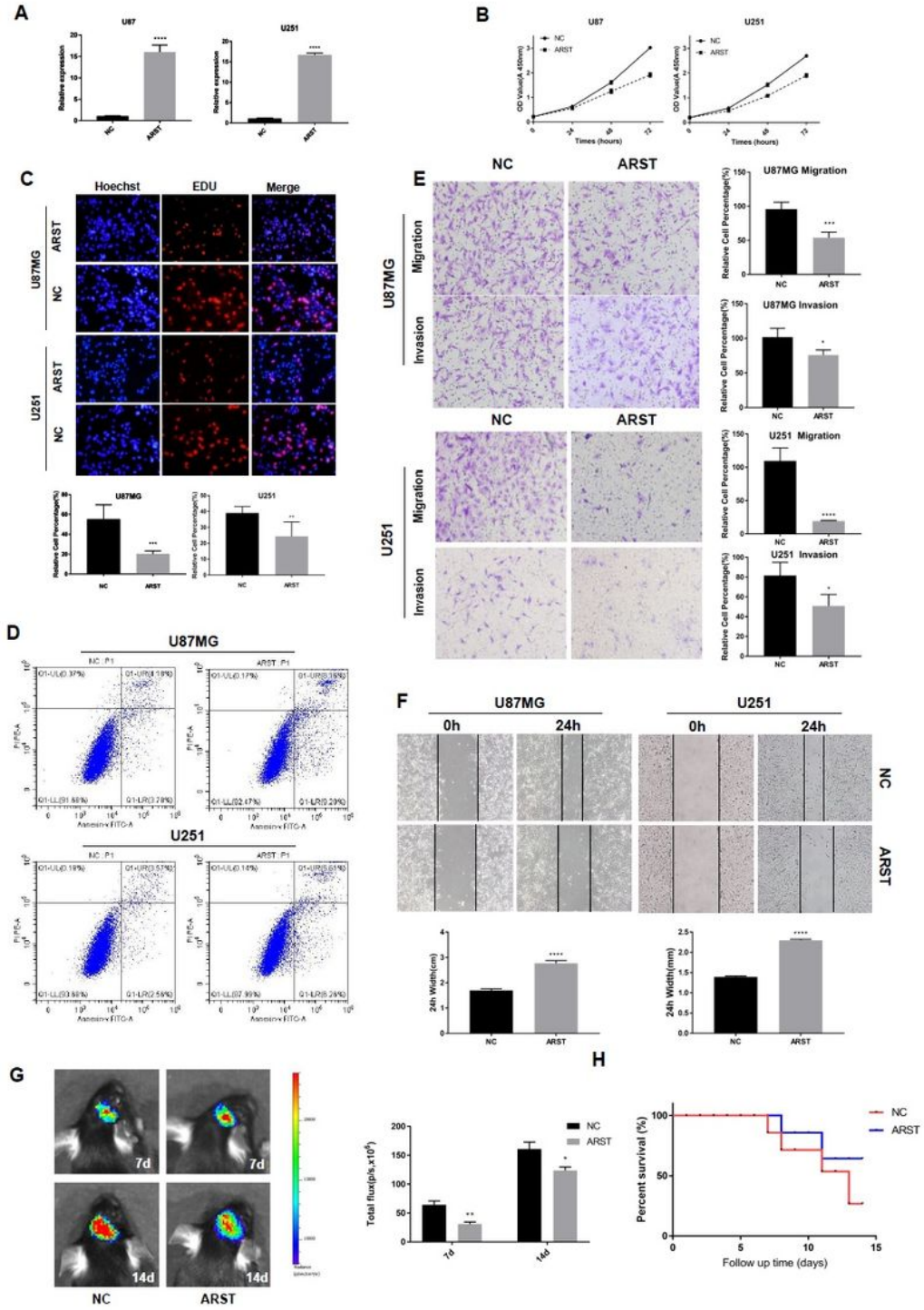


## Figure 2

ARST inhibited the malignant phenotypes of the glioma cells (A) The efficiencies of ARST overexpression in the U87MG and U251 cells were tested by qRT-PCR. Each bar represents mean ± s.d. from three independent experiments. (B) The growth curves of the transfected glioma cells were shown using CCK-8 assay. The results are presented as mean ± s.d. from three independent experiments. (C) An EdU staining assay was performed to determine the proliferation of the transfected U87MG and U251 cells. Data are

presented as mean ± s.d. from three independent experiments. (D) Apoptosis of the transfected cells were analyzed by duel staining of Annexin V and PI followed by flow cytometry assay. (E) Migration and invasion of the transfected cells were determined by transwell assay. Each bar represents mean ± s.d. from three independent experiments. (F) Wound-healing assay was performed. The data are presented as mean ± s.d. from three independent experiments. (G) Representative images and total flux of the C57 mice 7 days and 14 days after intracranial implantation of the GL261 cells transfected with luminance tagged ARST or control plasmids by IVIS spectrum. Each bar represents mean ± s.d. from three independent experiments. (H) Surviving curves of the C57 mice with xenographed tumors intracranially was recorded for 15 days. *P < 0.05, **P < 0.01, ***P < 0.005, ****P < 0.001.

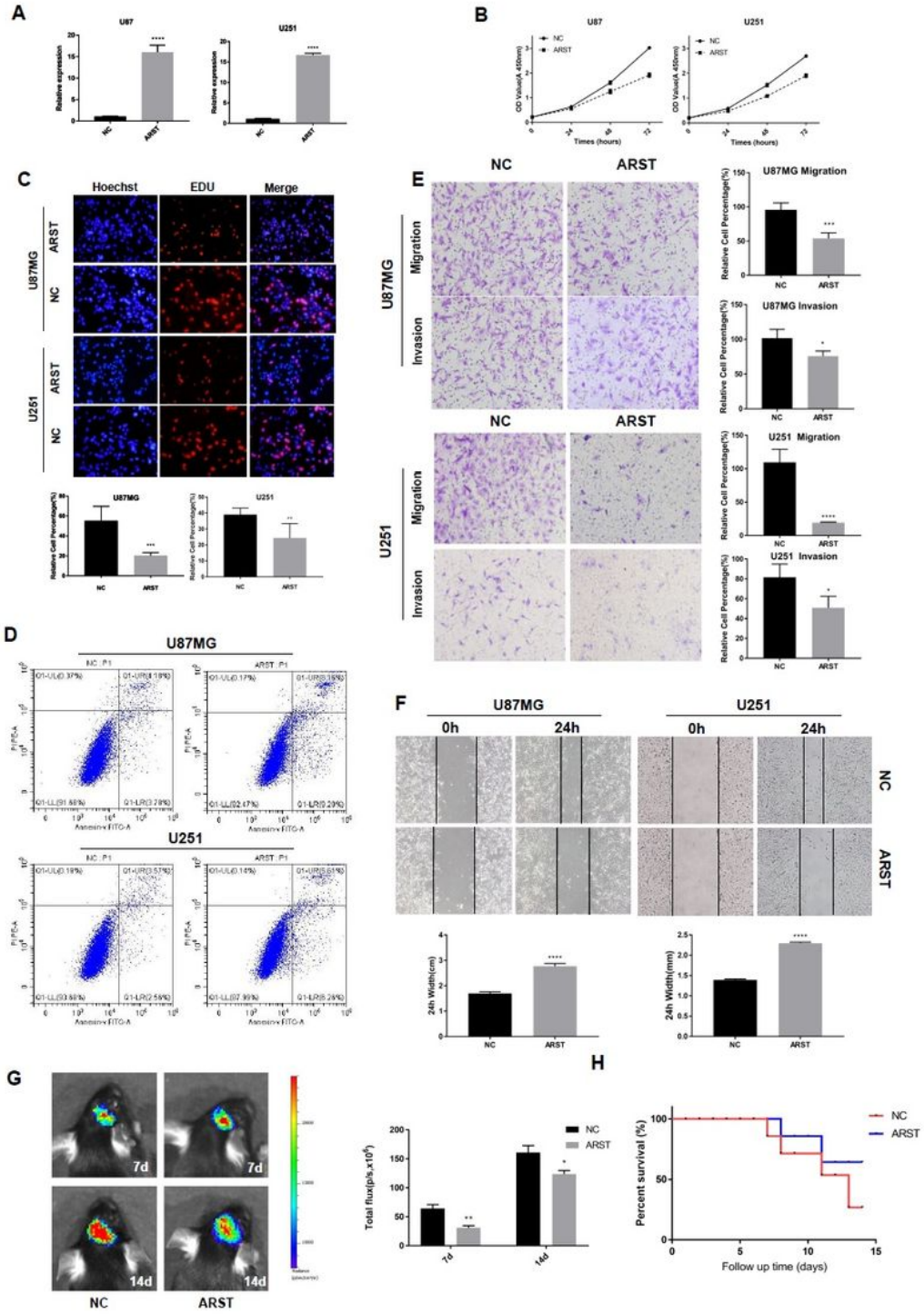


## Figure 2

ARST inhibited the malignant phenotypes of the glioma cells (A) The efficiencies of ARST overexpression in the U87MG and U251 cells were tested by qRT-PCR. Each bar represents mean ± s.d. from three independent experiments. (B) The growth curves of the transfected glioma cells were shown using CCK-8 assay. The results are presented as mean ± s.d. from three independent experiments. (C) An EdU staining assay was performed to determine the proliferation of the transfected U87MG and U251 cells. Data are

presented as mean ± s.d. from three independent experiments. (D) Apoptosis of the transfected cells were analyzed by duel staining of Annexin V and PI followed by flow cytometry assay. (E) Migration and invasion of the transfected cells were determined by transwell assay. Each bar represents mean ± s.d. from three independent experiments. (F) Wound-healing assay was performed. The data are presented as mean ± s.d. from three independent experiments. (G) Representative images and total flux of the C57 mice 7 days and 14 days after intracranial implantation of the GL261 cells transfected with luminance tagged ARST or control plasmids by IVIS spectrum. Each bar represents mean ± s.d. from three independent experiments. (H) Surviving curves of the C57 mice with xenographed tumors intracranially was recorded for 15 days. *P < 0.05, **P < 0.01, ***P < 0.005, ****P < 0.001.

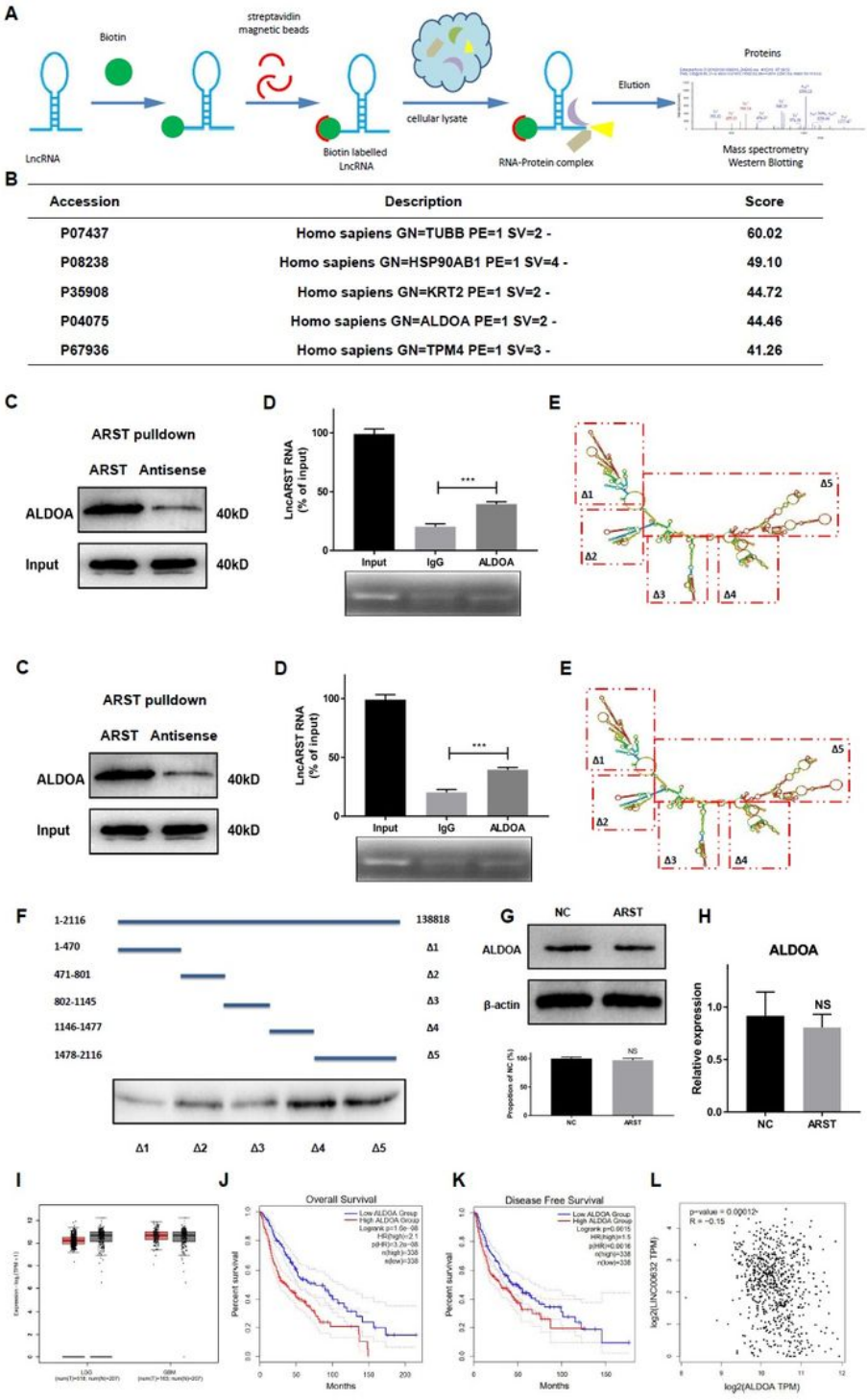


B

| Accession | Description | Score |
|---|---|---|
| P07437 | Homo sapiens GN=TUBB PE=1 SV=2 - | 60.02 |
| P08238 | Homo sapiens GN=HSP90AB1 PE=1 SV=4 - | 49.10 |
| P35908 | Homo sapiens GN=KRT2 PE=1 SV=2 - | 44.72 |
| P04075 | Homo sapiens GN=ALDOA PE=1 SV=2 - | 44.46 |
| P67936 | Homo sapiens GN=TPM4 PE=1 SV=3 - | 41.26 |



## Figure 3

LncRNA ARST interacted with ALDOA to exert its functions in glioma development (A) Sketch map of RNA pulldown followed by mass spectrometry assay to detect potential proteins interacting with ARST. (B) Potential binding proteins are listed based on the score of peptide identification from mass spectrometry assay. (C) Detection of ALDOA was conducted by Western blot from the purified proteins following RNA pulldown assay using biotinylated sense and antisense strands of ARST. (D) RNA

immunoprecipitation was performed to confirm the interaction between ARST and ALDOA in the U87MG cells. IgG was used as a negetive control. Data are presented as the mean±s.d. from three independent experiments. (E) ARST segmentation was displayed according to the loops of ARST 2D structure by red squares. (F) RNA pulldown followed by Western blot was performed to detect the binding affinity of ARST segments Δ1-Δ5 with ALDOA respectively. qRT-PCR (G) and Western blot (H) were performed to detect the expression levels of ALDOA in the cells upregulated with ARST compared to the control. Data are presented as mean ± s.d. from three independent experiments. (I) The expressions of ALDOA in the tissues from the patients with LGG or GBM in comparison to the normal persons based on the TCGA database. Overrall (J) and disease free (K) survivals of the glioma patients with low or high level of ALDOA expressions were assessed. (L) The correlation of the expressions between ALDOA and LINC00632 were displayed based on the TCGA database. *** P<0.005.

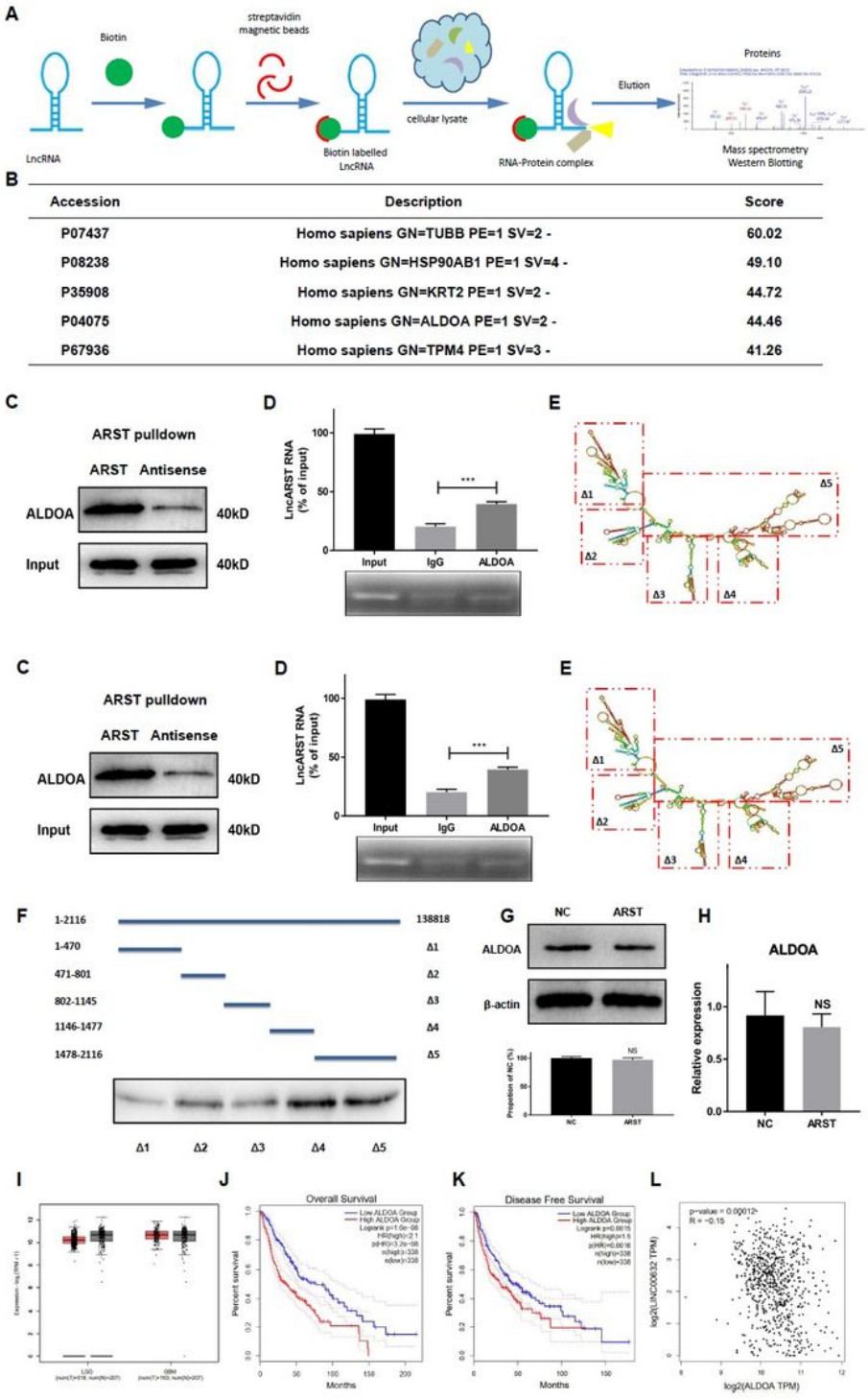


## Figure 3

LncRNA ARST interacted with ALDOA to exert its functions in glioma development (A) Sketch map of RNA pulldown followed by mass spectrometry assay to detect potential proteins interacting with ARST. (B) Potential binding proteins are listed based on the score of peptide identification from mass spectrometry assay. (C) Detection of ALDOA was conducted by Western blot from the purified proteins following RNA pulldown assay using biotinylated sense and antisense strands of ARST. (D) RNA

immunoprecipitation was performed to confirm the interaction between ARST and ALDOA in the U87MG cells. IgG was used as a negetive control. Data are presented as the mean±s.d. from three independent experiments. (E) ARST segmentation was displayed according to the loops of ARST 2D structure by red squares. (F) RNA pulldown followed by Western blot was performed to detect the binding affinity of ARST segments Δ1-Δ5 with ALDOA respectively. qRT-PCR (G) and Western blot (H) were performed to detect the expression levels of ALDOA in the cells upregulated with ARST compared to the control. Data are presented as mean ± s.d. from three independent experiments. (I) The expressions of ALDOA in the tissues from the patients with LGG or GBM in comparison to the normal persons based on the TCGA database. Overrall (J) and disease free (K) survivals of the glioma patients with low or high level of ALDOA expressions were assessed. (L) The correlation of the expressions between ALDOA and LINC00632 were displayed based on the TCGA database. *** P<0.005.

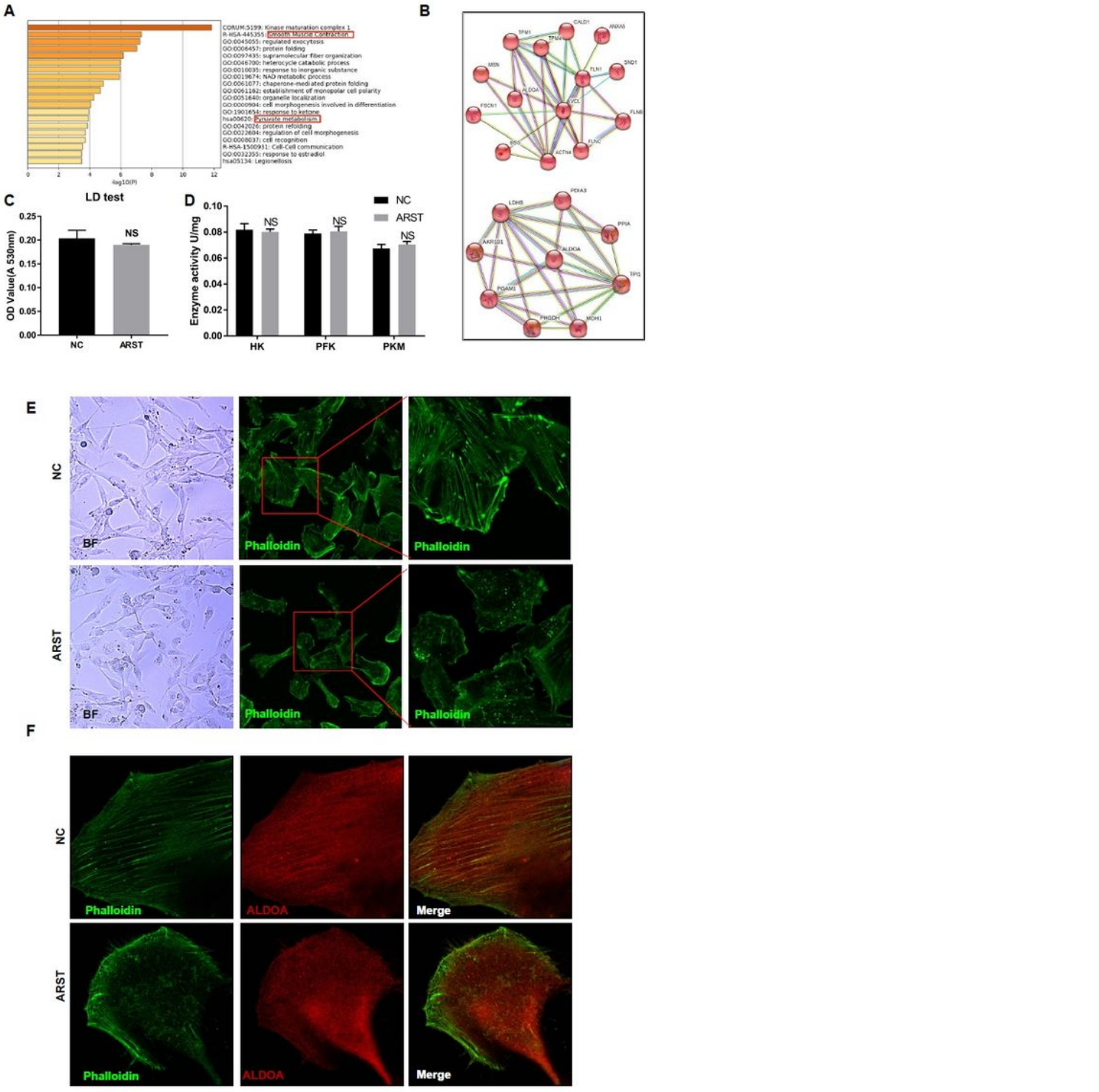


## Figure 4

ARST regulated ALDOA mediated actin filament integrity instead of its enzymatic activity (A) Core module correlation analysis of the proteins obtained in RNA-pulldown by mass spectrometry was performed on the Metascape database. ALDOA related functions were highlighted in red squares. (B) The networks of ALDOA interacting proteins involved in the ALDOA related functions were estimated by the String database. (C) Lactate production was measured in the U87 cells upregulated with ARST (ARST)

compared to the negative control (NC). Data are presented as mean ± s.d. from three independent experiments. (D) Enzymatic activities of HK, PKM and PFK were determined in the indicated cells. Each bar represents mean ± s.d. from three independent experiments. (E) Inverted phase (200X) and confocal laser scanning microscopes (630X) were utilized to observe the morphological changes of the transfected cells and the phalloidin stained F-actin cytoskeleton in them. (F) Dual staining of ALDOA and F-actin in the indicated cells was performed. Images were taken under confocal laser scanning microscope (630X).

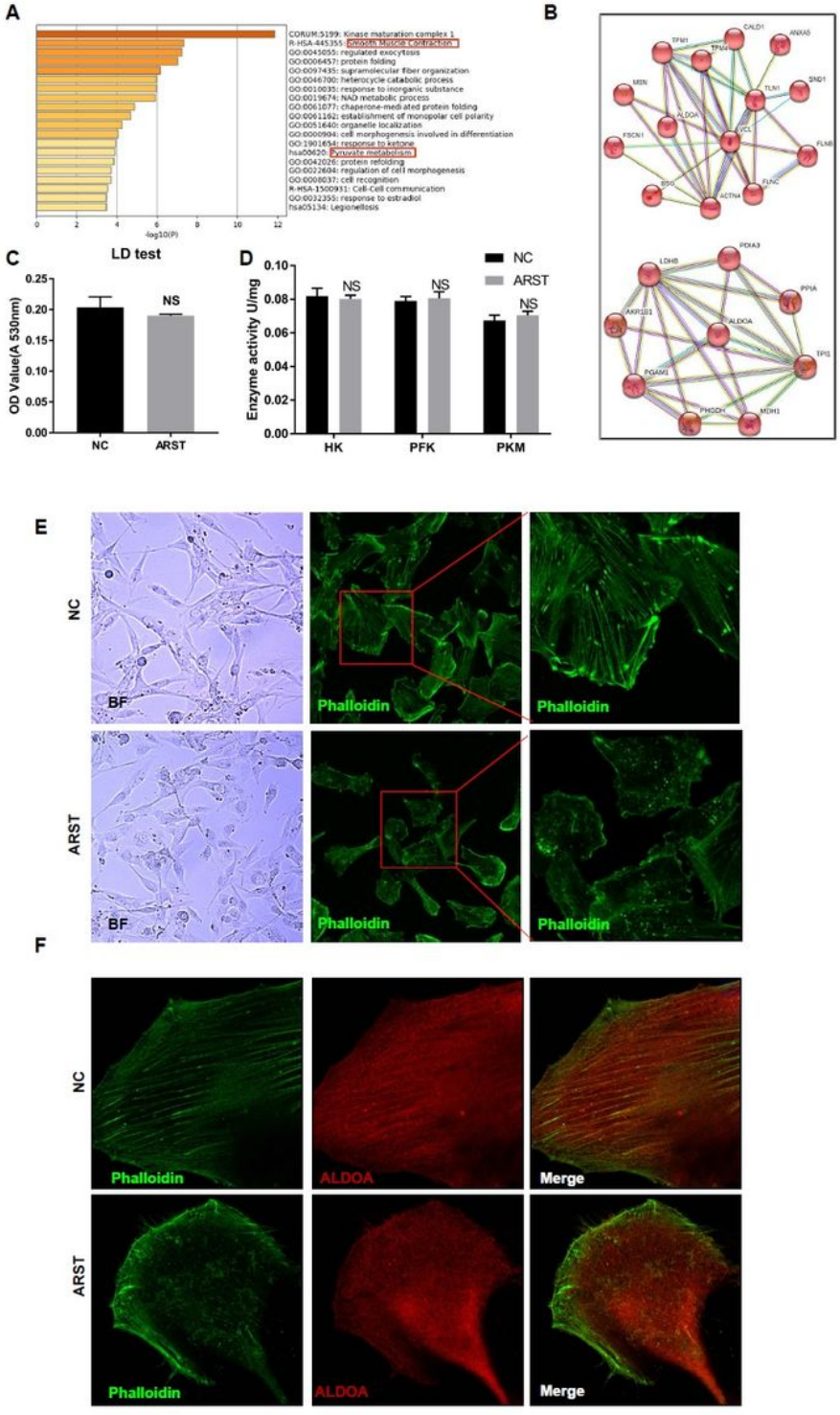

## Figure 4

ARST regulated ALDOA mediated actin filament integrity instead of its enzymatic activity (A) Core module correlation analysis of the proteins obtained in RNA-pulldown by mass spectrometry was performed on the Metascape database. ALDOA related functions were highlighted in red squares. (B) The networks of ALDOA interacting proteins involved in the ALDOA related functions were estimated by the String database. (C) Lactate production was measured in the U87 cells upregulated with ARST (ARST) compared to the negative control (NC). Data are presented as mean ± s.d. from three independent experiments. (D) Enzymatic activities of HK, PKM and PFK were determined in the indicated cells. Each bar represents mean ± s.d. from three independent experiments. (E) Inverted phase (200X) and confocal laser scanning microscopes (630X) were utilized to observe the morphological changes of the transfected cells and the phalloidin stained F-actin cytoskeloton in them. (F) Dual staining of ALDOA and F-actin in the indicated cells was performed. Images were taken under confocal laser scanning microscope (630X).

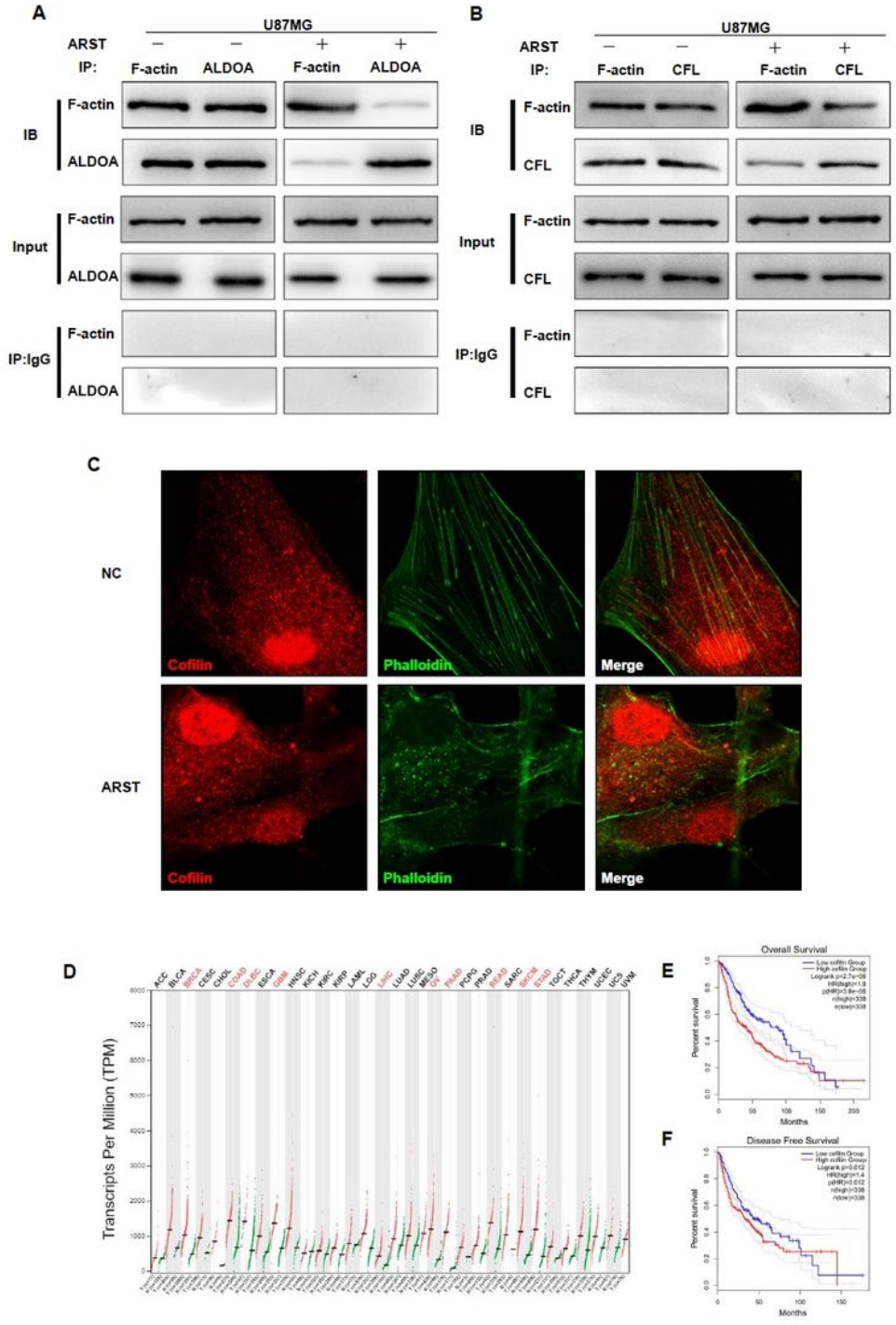


## Figure 5

ARST decreased the interactions of ALDOA and cofilin with F-actin, respectively (A,B) Co-immunoprecipitation assay was performed to detect the binding capacity of F-actin and ALDOA or cofilin in the U87 cells upregulated with ARST in comparison to the negative control. (C) Dual staining of cofilin and phalloidin labelled F-actin cytoskeloton was performed in the transfected cells. Images were taken under confocal laser scanning microscope (630X). (D) Transcripts per million (TPM) of cofilin in different

cancers based on the TCGA database. Overall (E) and disease free (F) survivals of the glioma patients with low or high level of cofilin expressions were assessed in the GEPIA database.

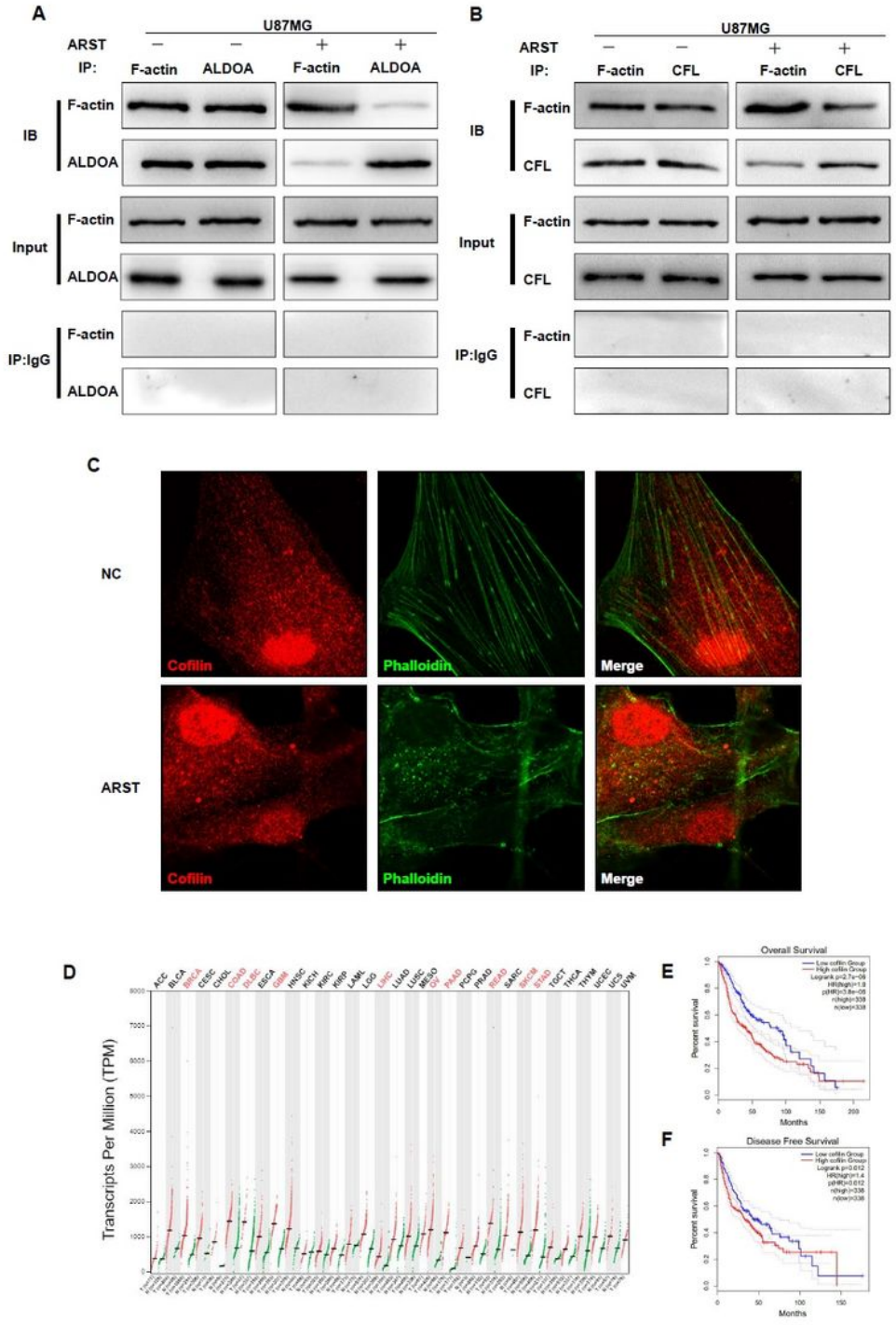


## Figure 5

ARST decreased the interactions of ALDOA and cofilin with F-actin, respectively (A,B) Co-immunoprecipitation assay was performed to detect the binding capacity of F-actin and ALDOA or cofilin in the U87 cells upregulated with ARST in comparison to the negative control. (C) Dual staining of cofilin

and phalloidin labelled F-actin cytoskeloton was performed in the transfected cells. Images were taken under confocal laser scanning microscope (630X). (D) Transcripts per million (TPM) of cofilin in different cancers based on the TCGA database. Overall (E) and disease free (F) survivals of the glioma patients with low or high level of cofilin expressions were assessed in the GEPIA database.

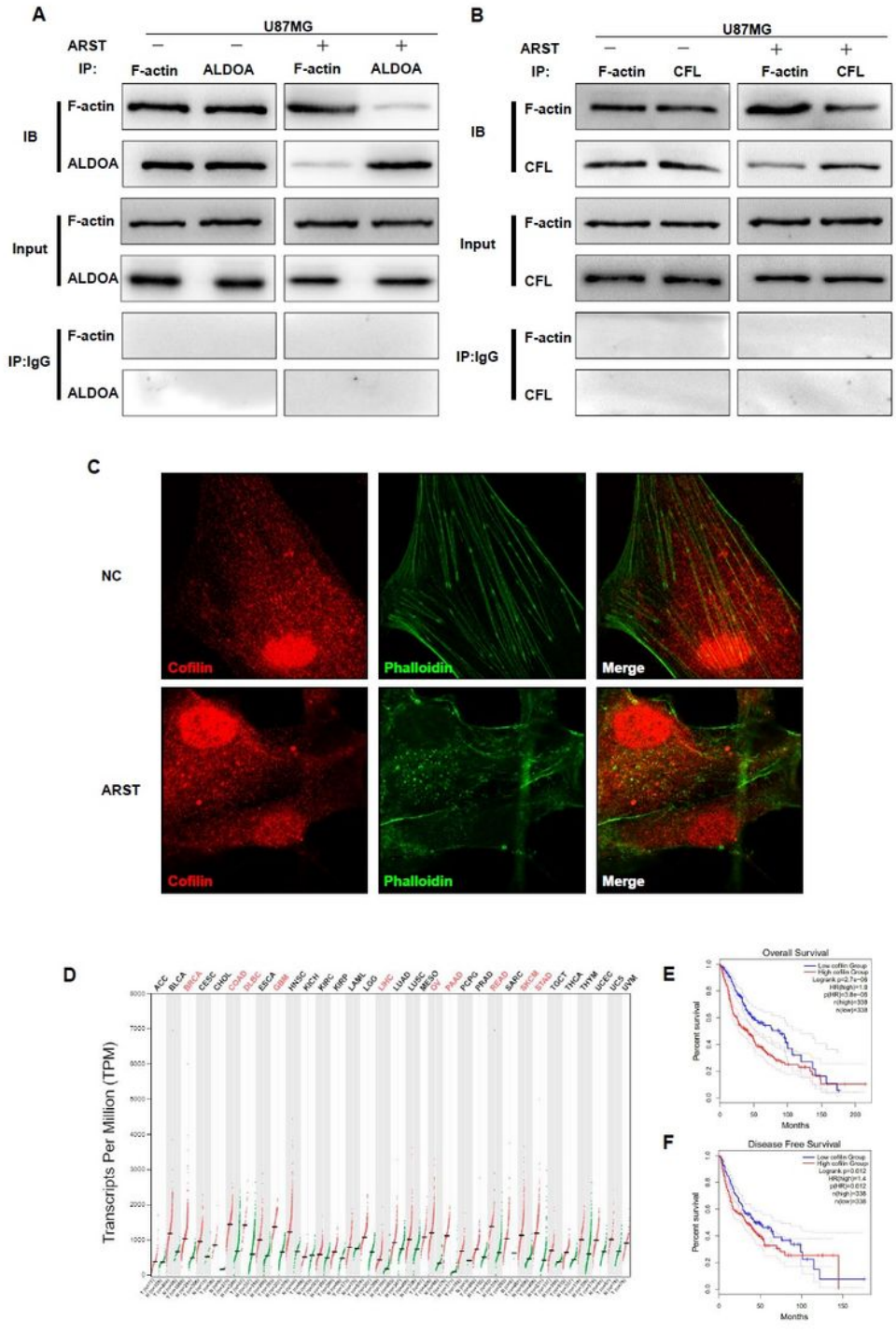


## Figure 5

ARST decreased the interactions of ALDOA and cofilin with F-actin, respectively (A,B) Co-immunoprecipitation assay was performed to detect the binding capacity of F-actin and ALDOA or cofilin in the U87 cells upregulated with ARST in comparison to the negative control. (C) Dual staining of cofilin and phalloidin labelled F-actin cytoskeloton was performed in the transfected cells. Images were taken under confocal laser scanning microscope (630X). (D) Transcripts per million (TPM) of cofilin in different cancers based on the TCGA database. Overall (E) and disease free (F) survivals of the glioma patients with low or high level of cofilin expressions were assessed in the GEPIA database.

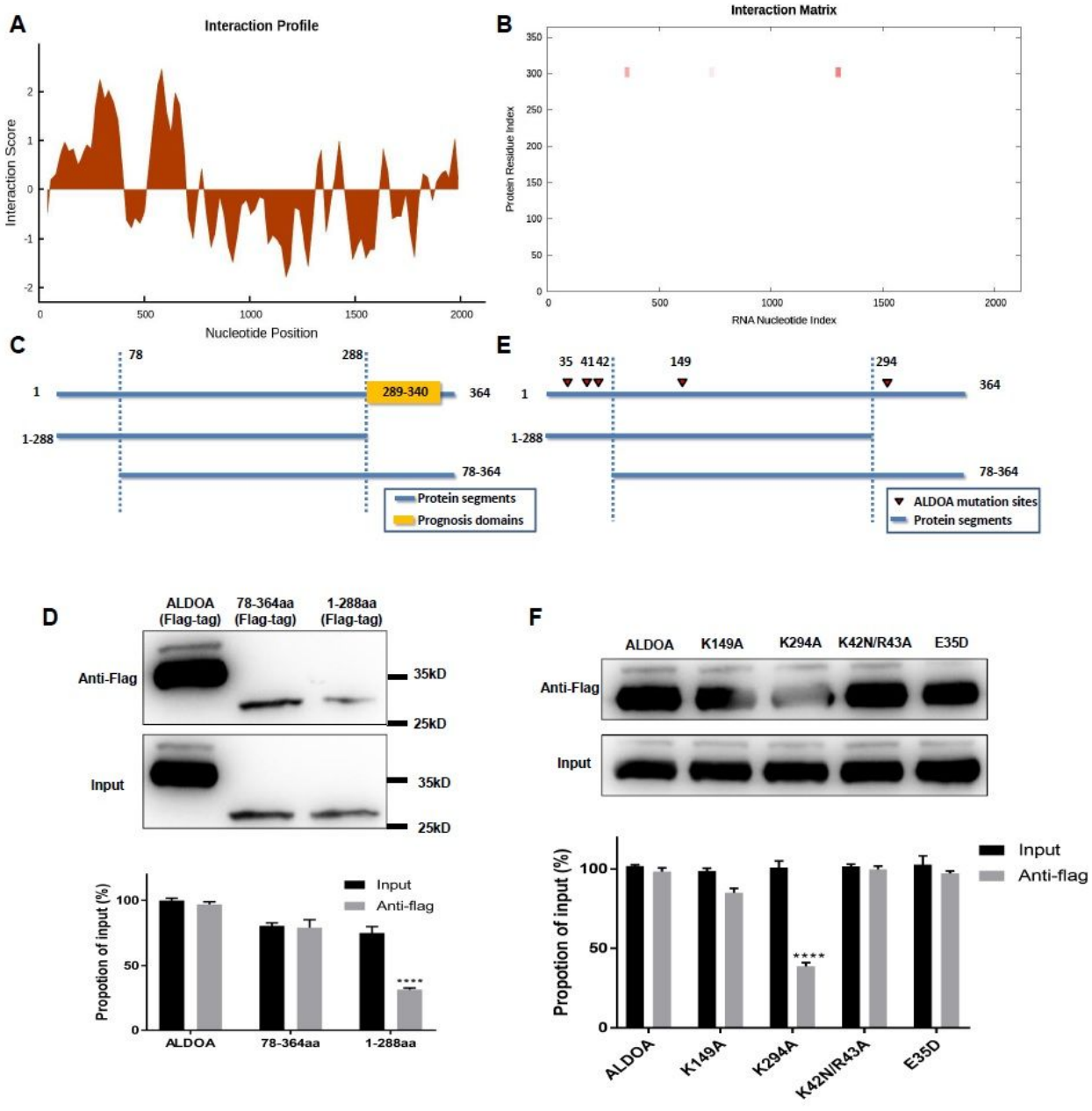


## Figure 6

ARST interacted with the binding sites of ALDOA and F-actin (A, B) CatRAPID database was referenced to predict the binding domains of ARST and ALDOA. (C) ARST segmentation is demonstrated by the diagrammatic sketch. The prognostic binding domain predicted by CatRAPID is highlighted in yellow. (D) RNA pulldown followed by Western blot was performed to detect the binding capacity of ALDOA segments with ARST. The results are presented as mean ± s.d. from three independent experiments. (E) The mutation sites on ARST, highlighted by red arrows, is demonstrated by diagrammatic sketch. (F) RNA pulldown followed by Western blot was performed to detect the interactive capacities of different mutant ALDOA with ARST. Each bar represents mean ± s.d. from three independent experiments. ****P <0.001.

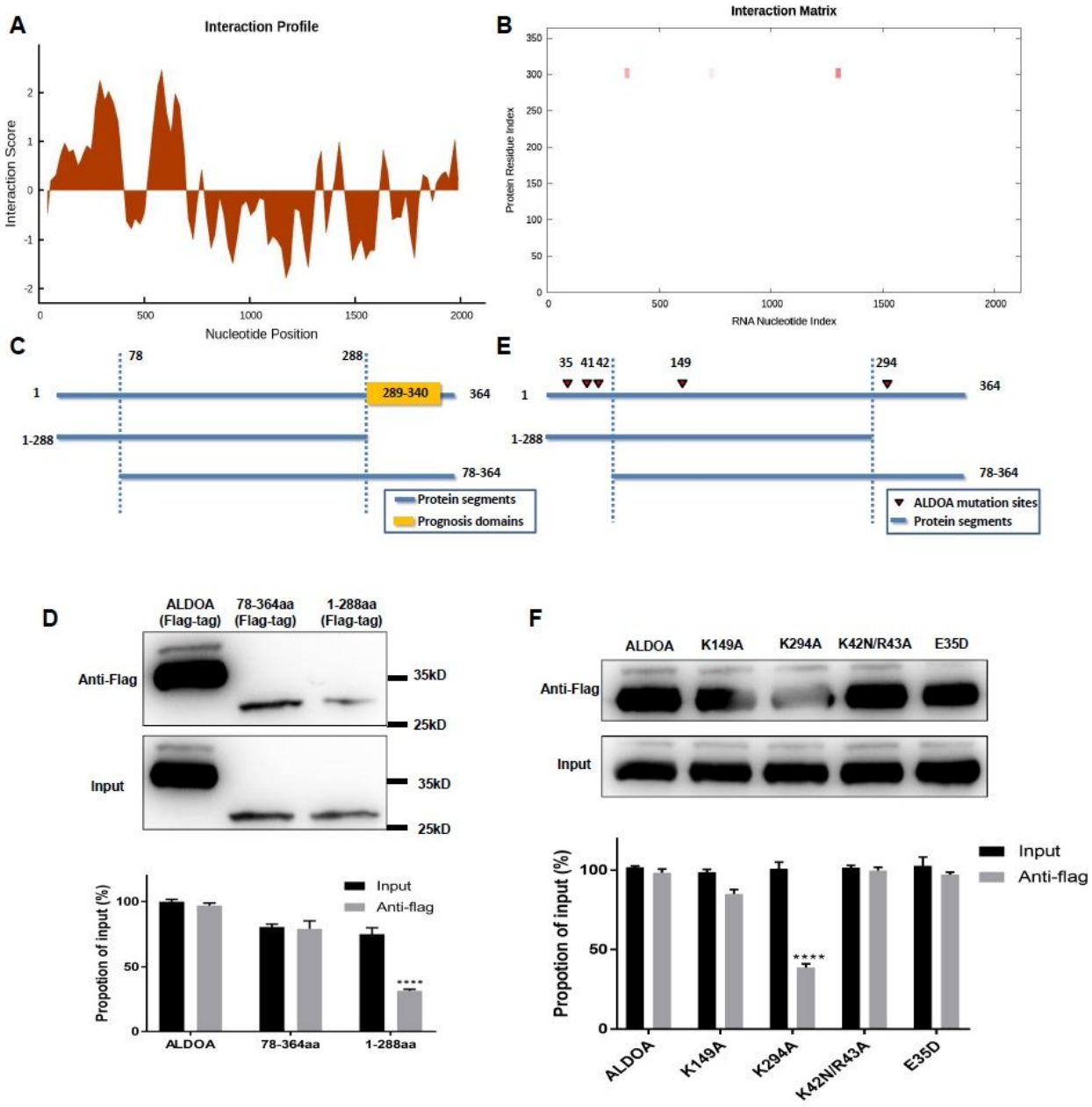


Figure 6

ARST interacted with the binding sites of ALDOA and F-actin (A, B) CatRAPID database was referenced to predict the binding domains of ARST and ALDOA. (C) ARST segmentation is demonstrated by the diagrammatic sketch. The prognostic binding domain predicted by CatRAPID is highlighted in yellow. (D) RNA pulldown followed by Western blot was performed to detect the binding capacity of ALDOA segments with ARST. The results are presented as mean ± s.d. from three independent experiments. (E) The mutation sites on ARST, highlighted by red arrows, is demonstrated by diagrammatic sketch. (F) RNA pulldown followed by Western blot was performed to detect the interactive capacities of different mutant ALDOA with ARST. Each bar represents mean ± s.d. from three independent experiments. ****P <0.001.

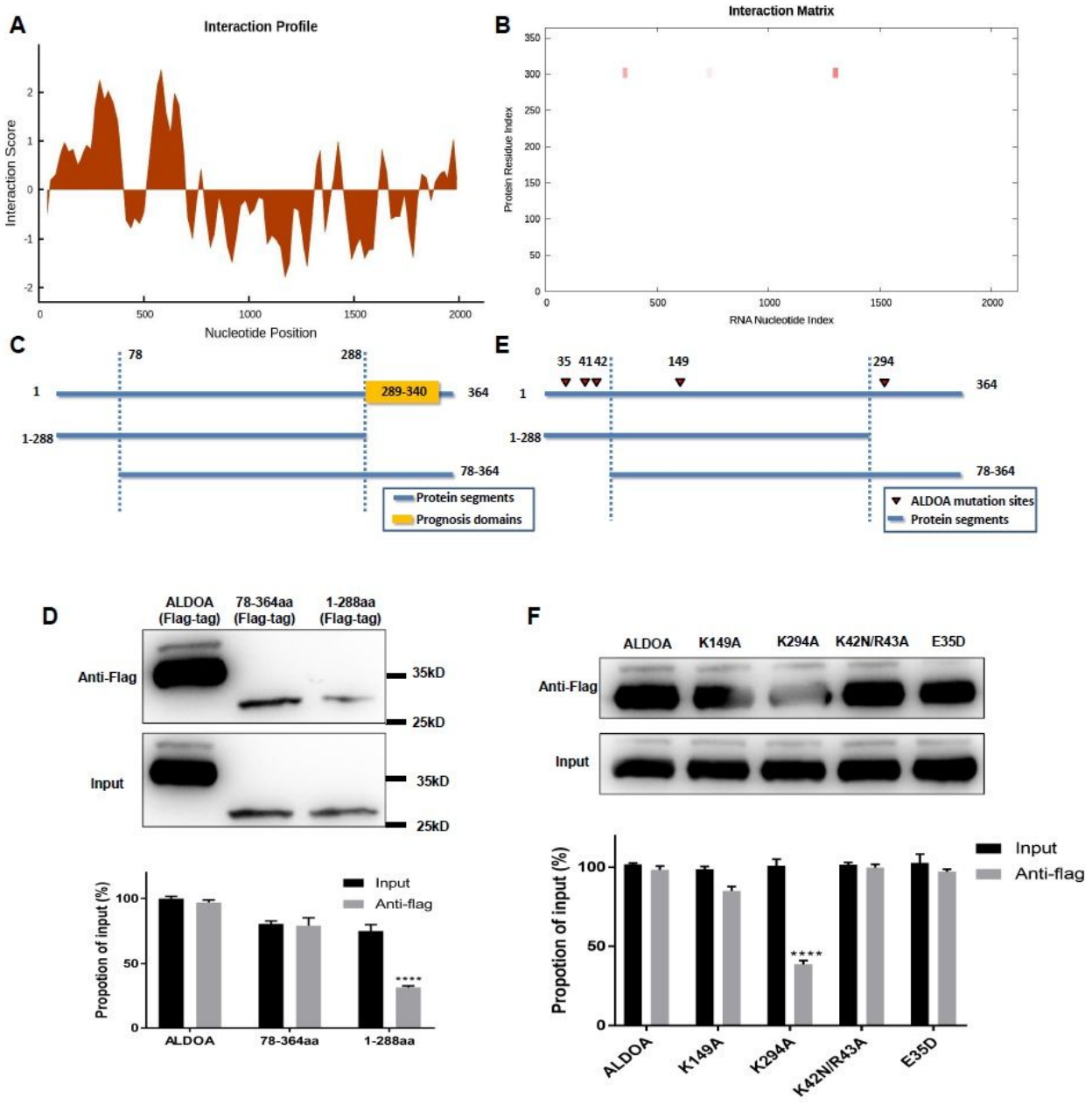


Figure 6

ARST interacted with the binding sites of ALDOA and F-actin (A, B) CatRAPID database was referenced to predict the binding domains of ARST and ALDOA. (C) ARST segmentation is demonstrated by the diagrammatic sketch. The prognostic binding domain predicted by CatRAPID is highlighted in yellow. (D) RNA pulldown followed by Western blot was performed to detect the binding capacity of ALDOA segments with ARST. The results are presented as mean ± s.d. from three independent experiments. (E) The mutation sites on ARST, highlighted by red arrows, is demonstrated by diagrammatic sketch. (F) RNA pulldown followed by Western blot was performed to detect the interactive capacities of different mutant ALDOA with ARST. Each bar represents mean ± s.d. from three independent experiments. ****P <0.001.

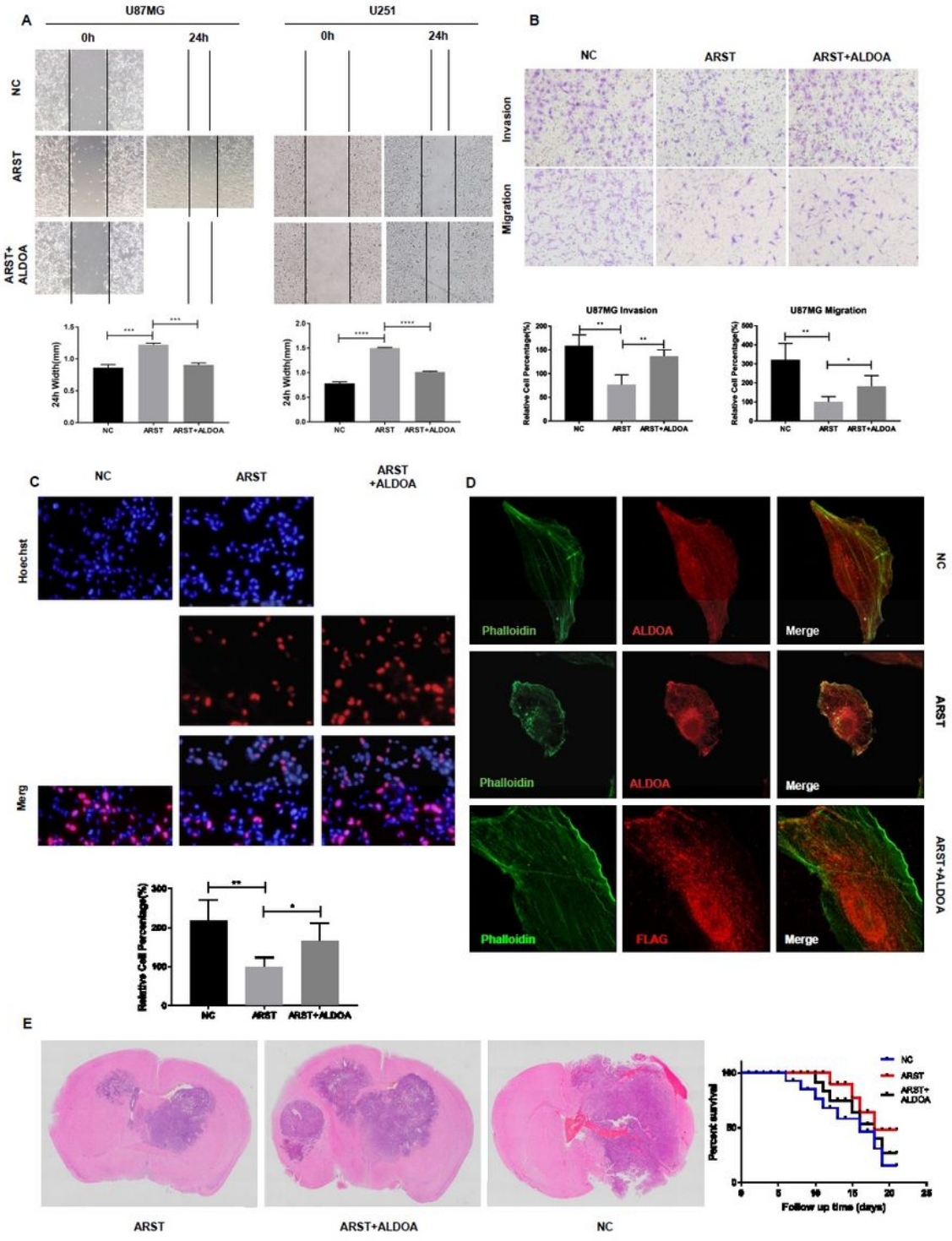


## Figure 7

Upregulation of ALDOA alleviated the inhibitory effects of ARST in gliomas The U87MG and U251 cells were transfected with the plasmids expressing empty vector (NC), ARST together with empty vector (ARST+vector), or ARST together with ALDOA (ARST+ALDOA). (A) Wound-healing assay was performed to detect the migrative abilities of the indictated cells. The results are presented mean ± s.d. from three independent experiments. (B) Migration and invasion of the transfected cells were determined by

transwell assay. Each bar represents mean ± s.d. from three independent experiments. (C) EdU assay was performed to detect the proliferation of the indicated cells. The data are presented as mean ± s.d. from three independent experiments. (D) Confocal laser scanning microscope was utilized to observe the dual staining of ALDOA and phalloidin labelled F-actin cytoskeloton in the indicated cells (630X). (E) Representative micrographs of H&E-stained sections of mouse brain tissues 15 days after intracranial implantation of the U87 cells transduced with a lentiviral vector expressing NC, ARST+vector or ARST+ALDOA. Curves show the survival rates of the engrafted mice. *P<0.05, **P<0.01, ***P<0.005, ****P<0.001.

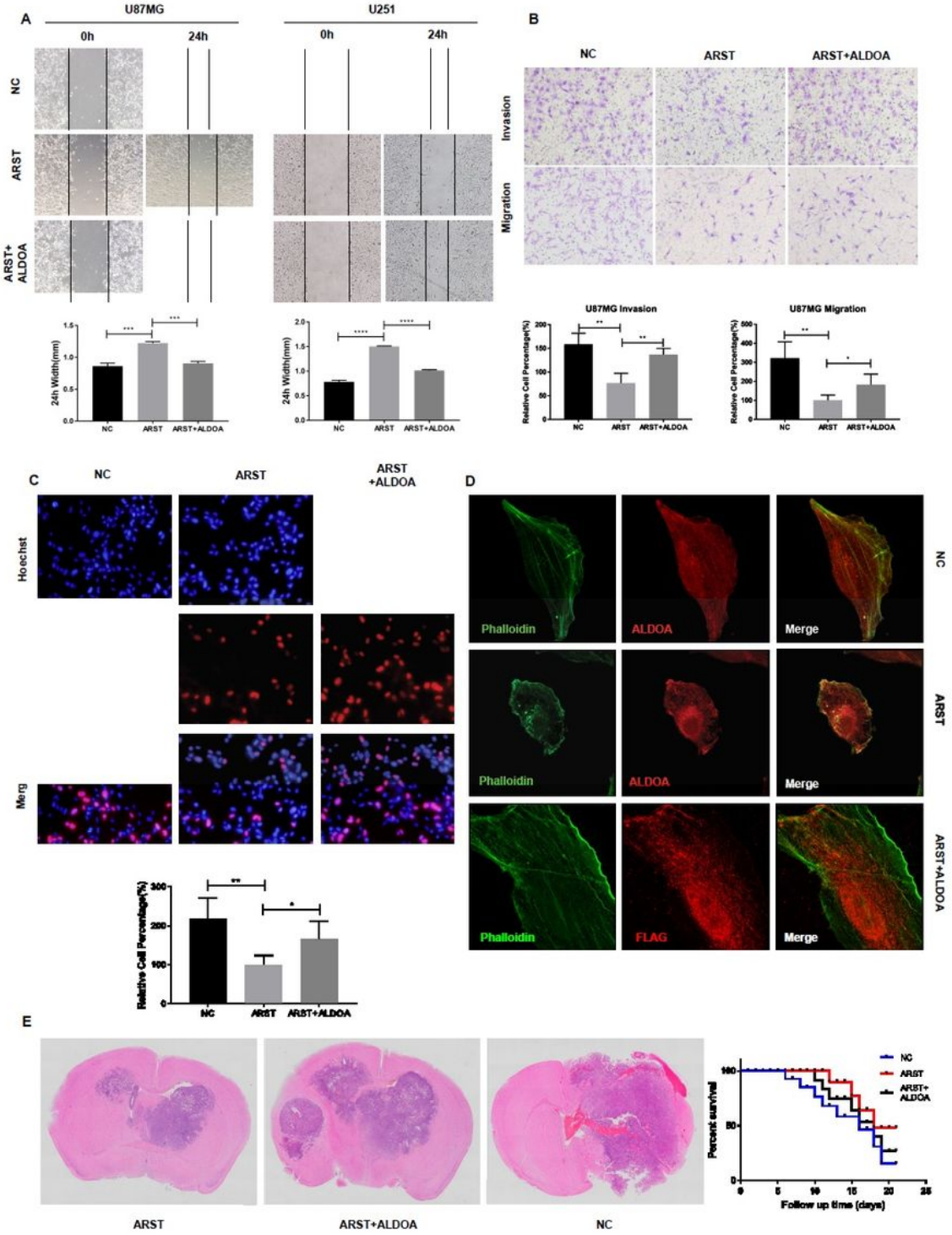


## Figure 7

Upregulation of ALDOA alleviated the inhibitory effects of ARST in gliomas The U87MG and U251 cells were transfected with the plasmids expressing empty vector (NC), ARST together with empty vector (ARST+vector), or ARST together with ALDOA (ARST+ALDOA). (A) Wound-healing assay was performed to detect the migrative abilities of the indictated cells. The results are presented mean ± s.d. from three independent experiments. (B) Migration and invasion of the transfected cells were determined by

transwell assay. Each bar represents mean ± s.d. from three independent experiments. (C) EdU assay was performed to detect the proliferation of the indicated cells. The data are presented as mean ± s.d. from three independent experiments. (D) Confocal laser scanning microscope was utilized to observe the dual staining of ALDOA and phalloidin labelled F-actin cytoskeloton in the indicated cells (630X). (E) Representative micrographs of H&E-stained sections of mouse brain tissues 15 days after intracranial implantation of the U87 cells transduced with a lentiviral vector expressing NC, ARST+vector or ARST+ALDOA. Curves show the survival rates of the engrafted mice. *P<0.05, **P<0.01, ***P<0.005, ****P<0.001.

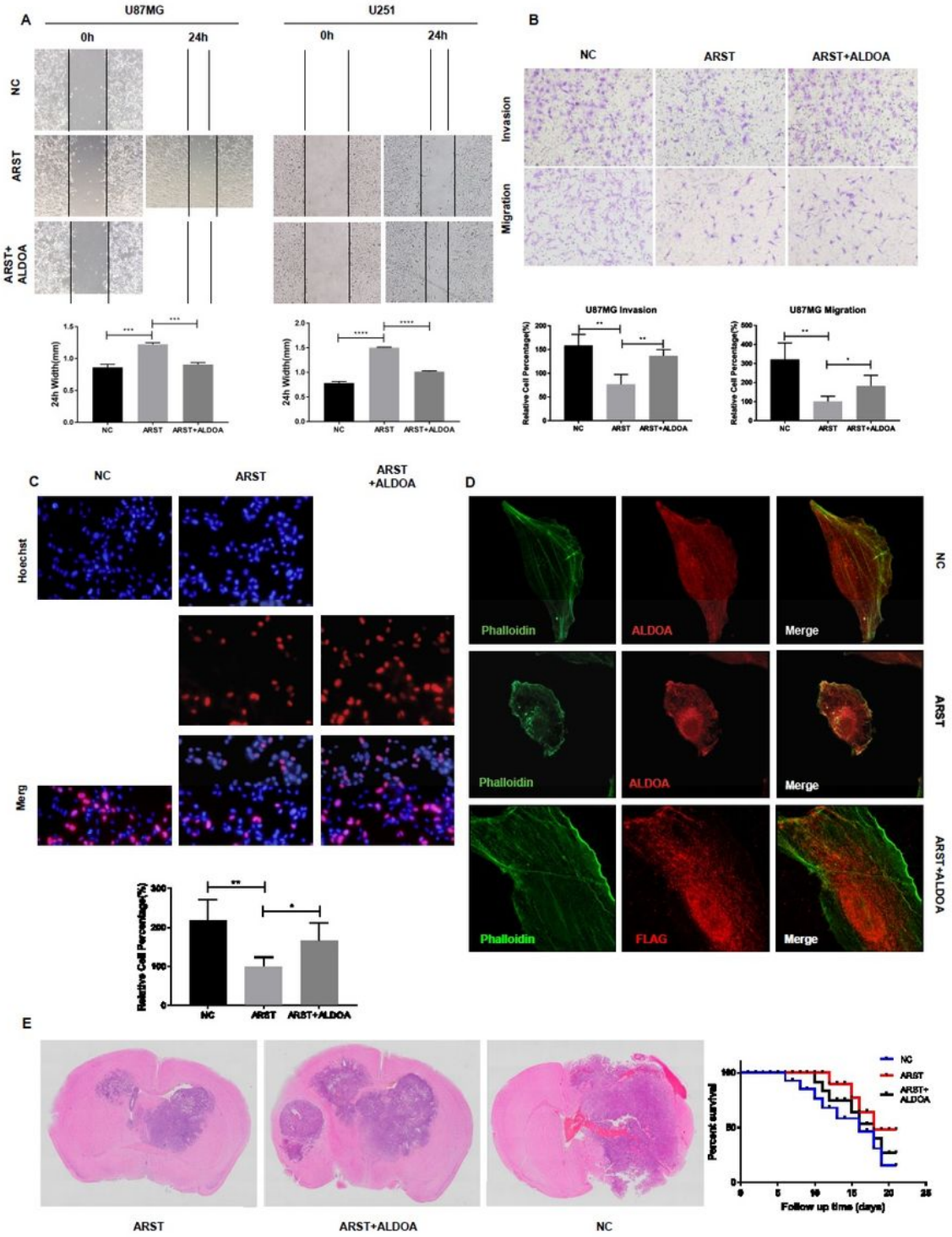


## Figure 7

Upregulation of ALDOA alleviated the inhibitory effects of ARST in gliomas The U87MG and U251 cells were transfected with the plasmids expressing empty vector (NC), ARST together with empty vector (ARST+vector), or ARST together with ALDOA (ARST+ALDOA). (A) Wound-healing assay was performed to detect the migrative abilities of the indictated cells. The results are presented mean ± s.d. from three independent experiments. (B) Migration and invasion of the transfected cells were determined by

transwell assay. Each bar represents mean ± s.d. from three independent experiments. (C) EdU assay was performed to detect the proliferation of the indicated cells. The data are presented as mean ± s.d. from three independent experiments. (D) Confocal laser scanning microscope was utilized to observe the dual staining of ALDOA and phalloidin labelled F-actin cytoskeloton in the indicated cells (630X). (E) Representative micrographs of H&E-stained sections of mouse brain tissues 15 days after intracranial implantation of the U87 cells transduced with a lentiviral vector expressing NC, ARST+vector or ARST+ALDOA. Curves show the survival rates of the engrafted mice. *P<0.05, **P<0.01, ***P<0.005, ****P<0.001.

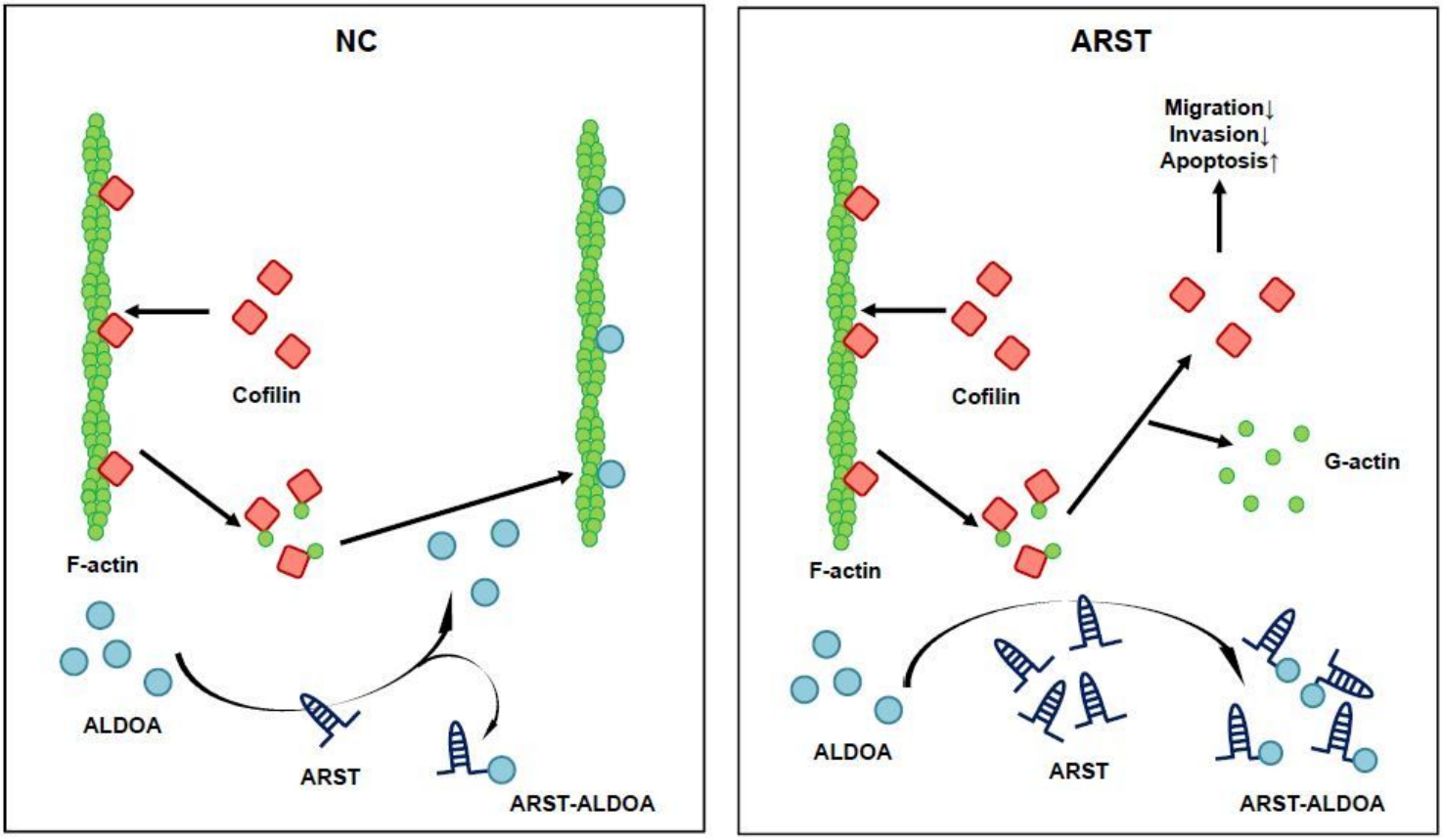


## Figure 8

Schematic model of ARST-mediated F-actin cytoskeleton modulation in gliomas

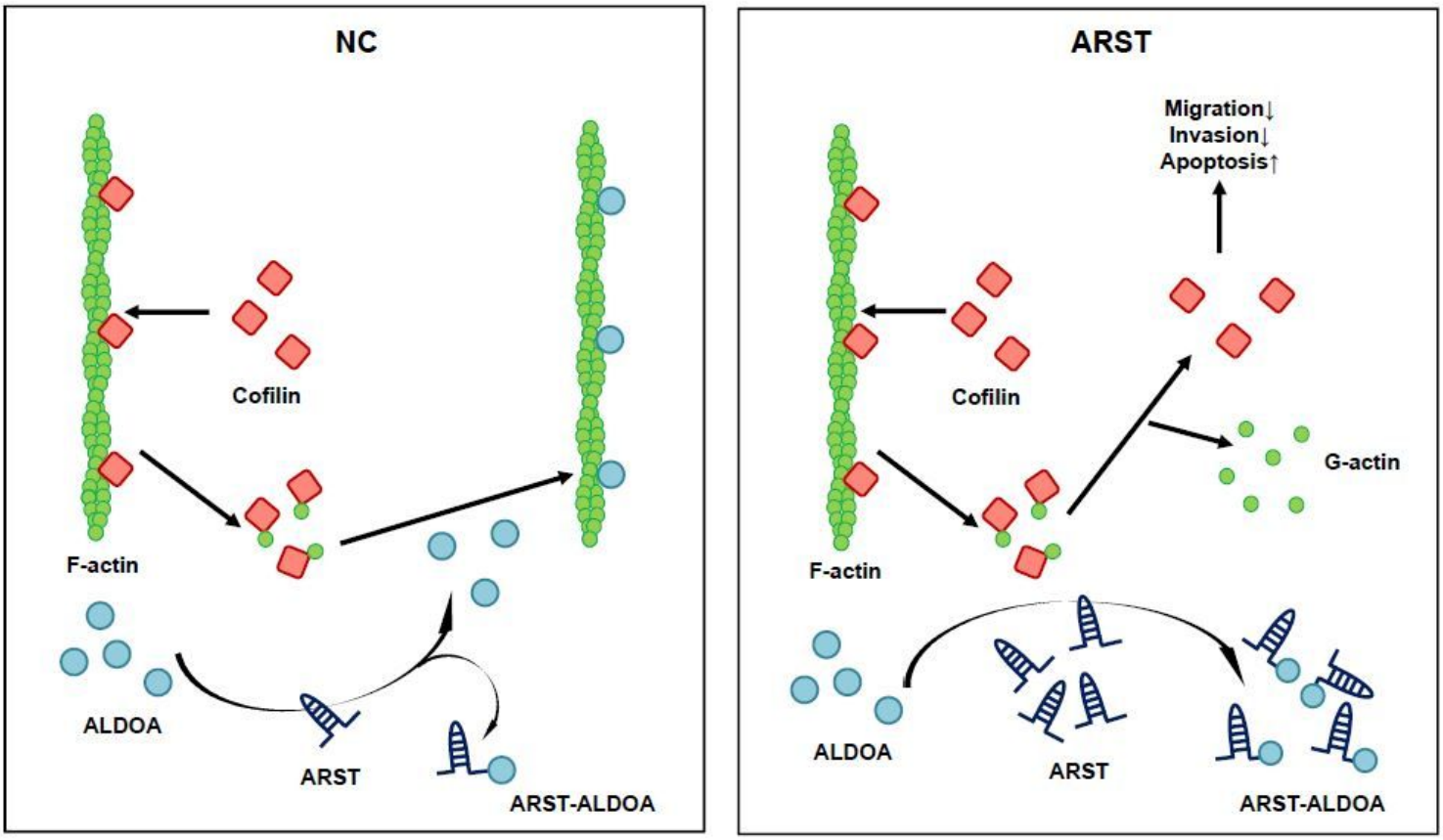


## Figure 8

Schematic model of ARST-mediated F-actin cytoskeleton modulation in gliomas

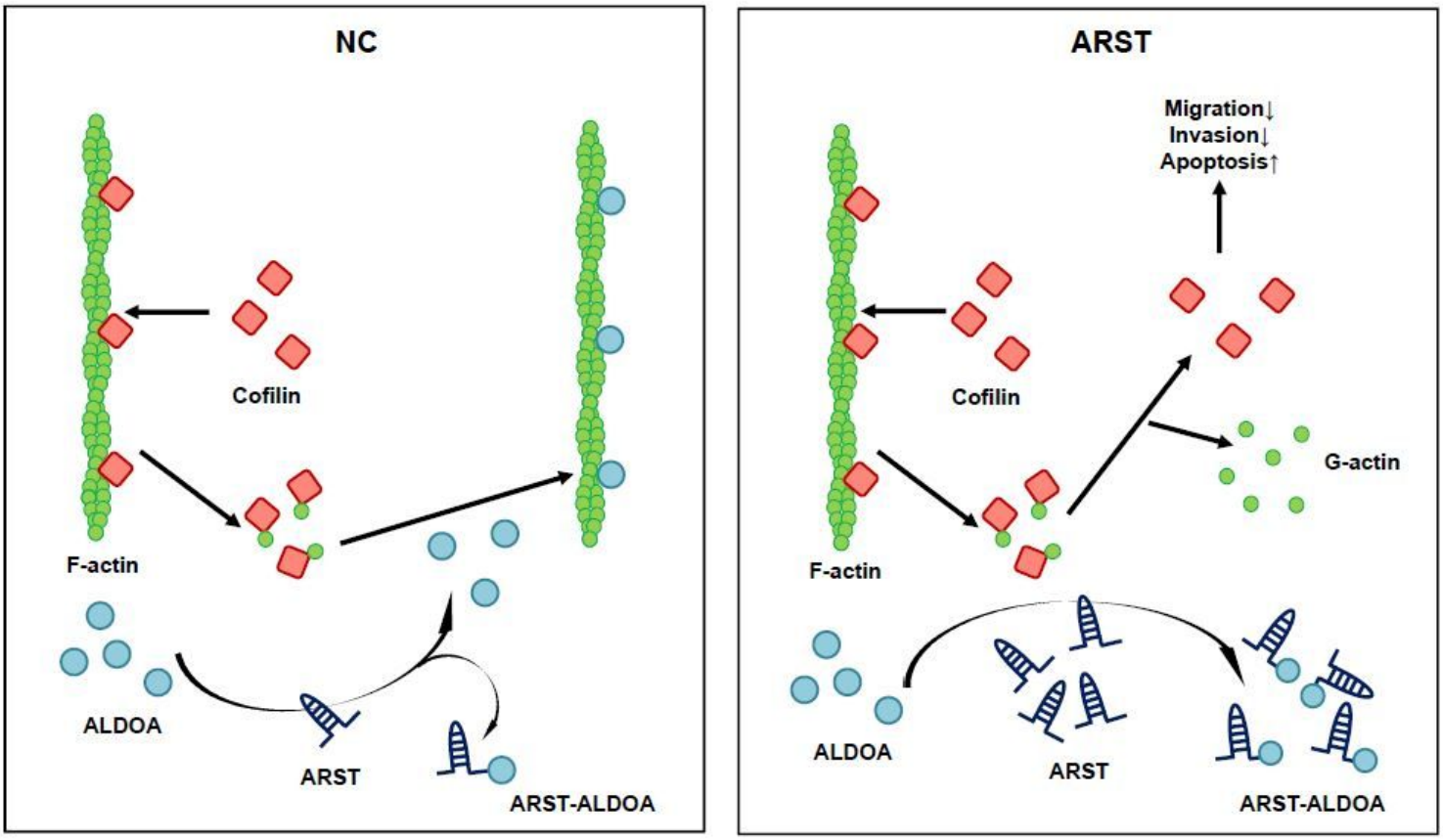


**Figure 8**

Schematic model of ARST-mediated F-actin cytoskeleton modulation in gliomas

## Supplementary Files

This is a list of supplementary files associated with this preprint. Click to download.

- Suppfigure1.pdf
- Suppfigure1.pdf
- Suppfigure2.pdf
- Suppfigure2.pdf
- Suppfigure2.pdf
- Suppfigure3.pdf
- Suppfigure3.pdf
- Supplementarytable1.xlsx
- Supplementarytable1.xlsx
- Supplementarytable1.xlsx
- Supplementarytable2.xlsx

- Supplementarytable2.xlsx
- Supplementarytable3.xlsx
- Supplementarytable3.xlsx
- Supplementarytable3.xlsx
- Supplementarytable4.xlsx
- Supplementarytable4.xlsx
- Supplementarytable4.xlsx
- suppfigure4.pdf
- suppfigure4.pdf
- Supplementaryimformation.docx
- Supplementaryimformation.docx
- Supplementaryimformation.docx